https://doi.org/10.5194/egusphere-2026-2380
Preprint. Discussion started: 8 May 2026

Assessing Air Pollution Drivers in Asia Through Multi-Species Data Assimilation During NASA's ASIA-AQ Campaign

Jinkyul Choi[1], Kazuyuki Miyazaki[1,2], Takashi Sekiya[3], Jinhyeok Yu[1], Shin-Ya Ogino[4], Henk Eskes[5], Pieter Rijdijk[5], Ryan Bennett[6], Anke Roiger[7], Leon Knez[7], Glenn S. Diskin[8], Jason A. Miech[8,9], Joshua P. DiGangi[8], Yonghoon Choi[8,10], Alessandro Franchin[11], Changmin Cho[11], Eric C. Apel[11], Louisa K. Emmons[11], Nattamon Maneenoi[12], Jason M. St. Clair[13,14], Reem A. Hannun[15], Glenn M. Wolfe[13], Erin Delaria[12], Abby Sebol[13], Donald R. Blake[16], Monica Crippa[17], Rachel M. Hoesly[18], Steven J. Smith[18,19], Jung-Hun Woo[20], Le Kuai[1,2], Ronald Macatangay[21]

[1] Jet Propulsion Laboratory, California Institute of Technology, Pasadena, CA, USA
[2] Joint Institute for Regional System Science and Engineering (JIFRESSE), University of California, Los Angeles, Los Angeles, CA, USA
[3] Japan Agency for Marine-Earth Science and Technology (JAMSTEC), Yokohama, Japan
[4] Japan Agency for Marine-Earth Science and Technology (JAMSTEC), Yokosuka, Japan
[5] Royal Netherlands Meteorological Institute (KNMI), De Bilt, Netherlands
[6] Bay Area Environmental Research Institute, NASA Ames Research Center, Moffett Field, CA, USA
[7] Deutsches Zentrum für Luft- und Raumfahrt (DLR), Institut für Physik der Atmosphäre, Oberpfaffenhofen, Germany
[8] NASA Langley Research Center, Hampton, VA, USA
[9] Oak Ridge Associated Universities, Oak Ridge, TN, USA
[10] Analytical Mechanics Associates, Hampton, VA, USA
[11] Atmospheric Chemistry Observations and Modeling Laboratory, National Center for Atmospheric Research (NCAR), Boulder, CO, USA
[12] Department of Atmospheric and Oceanic Sciences, University of California, Los Angeles, Los Angeles, CA, USA
[13] Atmospheric Chemistry and Dynamics Laboratory, NASA Goddard Space Flight Center, Greenbelt, MD, USA
[14] University of Maryland, Baltimore County, Baltimore, MD, USA
[15] Earth Science Division, NASA Ames Research Center, Moffett Field, CA, USA
[16] Department of Chemistry, University of California, Irvine, CA, USA
[17] European Commission, Joint Research Centre (JTC), Ispra, Italy
[18] Joint Global Change Research Institute, Pacific Northwest National Lab, College Park, MD, USA
[19] Department of Atmospheric and Oceanic Science, University of Maryland, College Park, MD, USA
[20] Department of Environmental Management, Seoul National University, Seoul, South Korea
[21] Center for Atmospheric Science Research, National Astronomical Research Institute of Thailand, Chiang Mai, Thailand

Correspondence to: Jinkyul Choi (jinkyul.choi@jpl.nasa.gov)

https://doi.org/10.5194/egusphere-2026-2380
Preprint. Discussion started: 8 May 2026

Abstract. Asia accounts for approximately half of global anthropogenic emissions of major pollutants, yet emission inventories remain uncertain and ground-based monitoring is sparse across much of the region. To address these challenges, this study applies a multi-species satellite data assimilation framework to estimate emissions and concentrations of key chemical species during the NASA's ASIA-AQ campaign. The assimilation improves agreement with airborne observations for O_3, NO_x, CO, and CH_2O, with the largest gains for CO (correlation increasing from 0.63–0.64 to 0.77) and CH_2O (biases reduced by 41–70%). Domain-wide, the optimized emissions show increases of 15% for NO_x and 9% for CO, and a 52% reduction in isoprene. Comparisons with multiple emission inventories reveal large discrepancies, with normalized standard deviation ranging from 11% for NO_x in mainland China to 68% for CO in Taiwan. Over Thailand, the assimilation increases fire emissions from 3.6 Tg (GFASv1.2) to 8.3 Tg, while FINNv2.7 produces estimates roughly twice as high, highlighting persistent divergence among fire emission estimates. Source-receptor analysis reveals strong meteorological control on transboundary pollutant: long-range transport contributes up to 62% of surface O_3 in Manila during strong monsoon conditions, whereas Seoul exhibits local NO_x-saturated chemistry. During a strong transport episode, Indian emissions account for 72–78% of the free tropospheric O_3 response over Taipei and Chiang Mai, and 24% over Seoul, highlighting an overlooked transport pathway affecting Asian air quality. These results highlight the value of satellite data assimilation and the need for improved inventories and coordinated action on local and transboundary pollution.

1 Introduction

Asian countries in the 2020s account for approximately half of the global anthropogenic emissions of major pollutants such as nitrogen oxides (NO_x), carbon monoxide (CO), and sulfur dioxide (SO_2) (Guizzardi et al., 2025), as well as carbon dioxide (CO_2) (Friedlingstein et al., 2023). This dominance reflects the region's dramatic development over the past three decades, characterized by surging energy consumption (Energy Institute, 2025), industrial expansion (UNIDO, 2025), and urbanization (UN, 2025). These anthropogenic sources are compounded by biomass burning and biogenic emissions that vary seasonally and interannually, modulated by land-use change and climate variability (Field et al., 2009; Reddington et al., 2014; Marlier et al., 2015; Peñuelas and Staudt, 2010). Consequently, emissions exhibit complex spatiotemporal heterogeneity, complicating efforts to attribute observed air quality (AQ) changes and to understand their underlying drivers across the region.

Air pollution governance across Northeast and Southeast Asia operates through a multi-layered architecture of United Nations (UN) agencies and regional intergovernmental bodies. Partnerships such as the Asia Pacific Clean Air Partnership (APCAP)

https://doi.org/10.5194/egusphere-2026-2380
Preprint. Discussion started: 8 May 2026

by the UN Environment Programme (UNEP) and the North-East Asia Clean Air Partnership (NEACAP) under the UN Economic and Social Commission for Asia and the Pacific (ESCAP) provide voluntary, science-based frameworks for policy exchange (UNEP, 2018; UN.ESCAP, 2025b). The Association of Southeast Asia Nations (ASEAN)'s Agreement on Transboundary Haze Pollution (AATHP), ratified by all ten member states, remains the region's only legally binding transboundary air pollution framework. The implementation of AATHP is supported by the ASEAN Zero-Burning Policy (ASEAN Secretariat, 2003) and the ASEAN Peatland Management Strategy targeting a haze-free ASEAN by 2030 (ASEAN Secretariat, 2023). Building on these frameworks, UN ESCAP adopted the Regional Action Programme on Air Pollution (RAPAP) in 2022 as the first region-wide action programme negotiated and agreed by governments to curb air pollution (UN.ESCAP, 2025a). Effective AQ management ultimately depends on national implementation, which varies considerably across the region.

At the national level, both China and South Korea have intensified efforts to mitigate air pollution through strengthened regulatory frameworks. Since 2013, China has implemented rigorous air pollution prevention and control action plans, achieving substantial reductions in NO_x and SO_2 emissions and ambient particulate matter (PM) concentrations (Zhang et al., 2019); however, surface ozone (O_3) pollution continued to increase due to nonlinear photochemistry (Liu et al., 2023; Ren et al., 2022). Similarly, South Korea's Clean Air Conservation Act in 2007 and the Special Act on the Improvement of Air Quality in Seoul Metropolitan Area in 2015 have effectively mitigated severe PM pollution, yet the country continues to face challenges with rising O_3 levels and remaining high $PM_{2.5}$ levels driven by complex secondary chemistry (Choi et al., 2024; Kim and Lee, 2018; Oak et al., 2025).

Countries in Southeast Asia have developed national AQ frameworks (Verma et al., 2023). The Philippines enacted the Philippine Clean Air Act (Republic Act No. 8749) in 1999, establishing national ambient AQ guideline values for criteria pollutants in 2000, with $PM_{2.5}$ standards tightened to 35 μg/m³ (24-hour) in 2020. Euro 4 vehicle emission standards have been mandatory since 2016, with Euro 5 scheduled for 2027. Limited studies indicate rising surface O_3 trends in the southern Philippines (Salvador et al., 2021) and persistent $PM_{2.5}$ exceedances in Metro Manila (Cruz et al., 2023; Hopke et al., 2008; Pabroa et al., 2022; Tseng et al., 2021), suggesting that current policies have not fully mitigated AQ. In Thailand, national ambient AQ standards were first issued in 1995, and $PM_{2.5}$ standards were revised in 2023 to 37.5 μg/m³ (24-hour), with Euro 5 becoming mandatory for new light-duty vehicles in 2024. Air quality management in Thailand has historically emphasized open burning control, yet Northern Thailand continues to experience severe seasonal pollution episodes driven by forest and agricultural burning and transboundary haze, indicating that biomass burning emissions remain significant despite existing policies (Phairuang et al., 2017, 2019; Song et al., 2022; Thongsame et al., 2025). $PM_{2.5}$ levels remain above both national standards and World Health Organization (WHO) guidelines (Nikam et al., 2021), and surface O_3 increased between 2000 and 2019 (Kittipornkul et al., 2023; Sukkhum et al., 2022).

https://doi.org/10.5194/egusphere-2026-2380
Preprint. Discussion started: 8 May 2026

Nevertheless, effective AQ management in the region is constrained by several fundamental challenges. First, the ground-based monitoring network is insufficient to fully characterize regional AQ. Regional monitoring is supported by ground-based networks such as the Acid Deposition Monitoring Network in East Asia (EANET) (EANET, 2021), remote sensing observations from Geostationary Environment Monitoring Spectrometer (GEMS) (Kim et al., 2020) and the Pandora Network (https://www.pandonia-global-network.org), and international research initiatives such as the Task Force on Hemispheric Transport of Air Pollution (TF HTAP) (Huang et al., 2017) and the Model Inter-comparison Study for Asia (MICS-Asia) (Itahashi et al., 2020), which further advance understanding of transboundary pollution. While some regions (e.g., eastern China, South Korea, and the Bangkok Metropolitan Region in Thailand) possess dense networks, vast areas in Southeast Asia lack sufficient observation sites, limiting our ability to monitor surface air quality (Martin et al., 2019; Sokhi et al., 2022). For example, in the Philippines, despite maintaining over 100 monitoring stations nationwide, the network remains largely concentrated in the National Capital Region, with limited real-time public reporting. In Thailand, the Pollution Control Department operates over 180 continuous monitoring stations across 65 provinces through the Air4Thai network, including approximately 90 in the Bangkok Metropolitan Region, yet coverage remains uneven across rural and northern provinces.

Second, bottom-up emission inventories, constructed using statistical activity data and emission factors for each sector, have inherent limitations. Reported emissions differ substantially across inventories, by more than a factor of 2 for anthropogenic emissions at the country level (Elguindi et al., 2020; Hoesly et al., 2018), factors of 2 to 3 for biomass burning emissions at the regional annual scale (van der Werf et al., 2017; Wiedinmyer et al., 2023), and factors of 2 to 3 for biogenic emissions at the global and regional annual scale (Guenther et al., 2012; Sindelarova et al., 2014, 2022). These uncertainties are particularly pronounced in Southeast Asia, where biomass burning inventories are largely uncertain due to limited burned area detection due to persistent cloud cover, as well as uncertain local activity data and emission factors (Kurokawa and Ohara, 2020; Stavrakou et al., 2014; Vongruang et al., 2017). In addition, most bottom-up inventories cannot be updated rapidly enough to represent short-term and spatially heterogeneous changes driven by evolving environmental policies, dynamic economic shifts, and climate variability.

Third, AQ in the region reflects both local emissions and substantial transboundary transport (Crawford et al., 2021). Consequently, domestic mitigation strategies alone are sometimes insufficient. Achieving national AQ targets may require a regional coordination and quantitative attribution of cross-border contributions.

To address the limitation of ground-based observations, satellite remote sensing provides continuous and wide-area observations. Low Earth Orbit (LEO) sensors have provided a global coverage of key pollutants and their precursors. These include the Ozone Monitoring Instrument (OMI) (Levelt et al., 2018), the Global Ozone Monitoring Experiment-2 (GOME-2) (Chan et al., 2023), the MODerate resolution Imaging Spectroradiometer (MODIS) (Pagano and Durham, 1993), the Visible Infrared Imaging Radiometer Suite (VIIRS) (Cao et al., 2014), the Measurements of Pollution in the Troposphere (MOPITT)

https://doi.org/10.5194/egusphere-2026-2380
Preprint. Discussion started: 8 May 2026

instrument (Deeter et al., 2017), and the TROPOspheric Monitoring Instrument (TROPOMI) (Veefkind et al., 2012). More recently, GEMS, a geostationary satellite, provides hourly observations over Asia (Kim et al., 2020). To integrate these satellite observations and to provide comprehensive information on atmospheric composition variability (Bocquet et al., 2015; Bousserez et al., 2016; Lahoz and Schneider, 2014; Mizzi et al., 2016), chemical data assimilation systems have been developed, enabling long-term chemical reanalysis (Inness et al., 2019; Miyazaki et al., 2015). Chemical data assimilation can also be used to derive emission estimates while optimizing broad atmospheric composition fields. The Tropospheric Chemistry Reanalysis version 2 (TCR-2) (Miyazaki et al., 2020b) was developed within the Multi-mOdel Multi-cOnstituent Chemical data assimilation (MOMO-Chem) framework (Miyazaki et al., 2020a), which has successfully demonstrated the capacity to provide chemically and dynamically consistent fields by correcting model biases through observational constraints.

While satellites are useful for estimating emissions, relating these measurements to surface AQ remains challenging due to satellites' reduced sensitivity toward the surface and uncertainties in vertical distribution. Sub-orbital observations from aircraft campaigns fill this critical gap by providing detailed vertical profiles of atmospheric composition. NASA's Airborne and Satellite Investigation of Asian Air Quality (ASIA-AQ) campaign was conducted in February and March 2024 to address these challenges in the Asian region. The campaign deployed the NASA DC-8 aircraft for 16 research flights across the Philippines, Taiwan, South Korea, and Thailand, obtaining comprehensive vertical profiles of trace gases and aerosols. These observations provide valuable data for validating satellite products and chemical reanalysis systems, quantifying emissions, and improving our understanding of pollution sources and transport processes in Asia.

In this study, we utilize the MOMO-Chem framework to comprehensively assess the origins of Asian air pollutants during the ASIA-AQ campaign. Tropospheric Chemistry Reanalysis version 3 (TCR-3), constructed through the assimilation of multi-species satellite retrievals, including NO_2, SO_2, formaldehyde (CH_2O), CO, O_3 and nitric acid (HNO_3), provides a comprehensive dataset of atmospheric composition and top-down emission estimates. Section 2 describes the methodology. Section 3 validates the chemical reanalysis against extensive in situ measurements acquired during the ASIA-AQ campaign. Section 4 characterizes emissions of air pollutant precursors constrained by satellite observations and compares them with bottom-up inventories. Section 5 quantifies the contribution of transboundary transport to O_3 using a source–receptor analysis based on the optimized emissions. Section 6 summarizes the main findings.

2 Methodology

2.1. Tropospheric chemistry reanalysis

The TCR-3 product, generated using the MOMO-Chem framework, is used in this study (Miyazaki et al., 2020a, 2020b). It employs an ensemble-based data assimilation system based on the Local Ensemble Transform Kalman Filter (LETKF) (Hunt

https://doi.org/10.5194/egusphere-2026-2380
Preprint. Discussion started: 8 May 2026

et al., 2007). The state vector includes various chemical concentrations as well as surface emissions of CO, NO_x, SO_2, and isoprene, as well as lightning production of NO_x, with background error covariance linking observed atmospheric concentrations to emission adjustments for each model grid cell.

The forecast model used is MIROC-Chem (Watanabe et al., 2011; Sekiya et al., 2018), a global chemistry–climate model that simulates coupled tropospheric and stratospheric chemistry, tracer transport, and wet and dry deposition. The model is configured with a horizontal resolution of approximately 1.125° × 1.125° (T106) and 32 vertical levels extending from the surface to 4.4 hPa. The model explicitly represents 92 chemical species and 262 chemical reactions, including the oxidation of non-methane volatile organic compounds (NMVOCs). The meteorological fields simulated by the MIROC-AGCM were nudged to 6-hourly ERA5 reanalysis (Hersbach et al., 2020). Compared to the previous reanalysis (TCR-2), TCR-3 utilizes updated inventories as prior emissions. Biomass burning emissions used in this study are from the Global Fire Assimilation System version 1.2 (GFASv1.2) (Kaiser et al., 2012). Anthropogenic emissions are from the Hemispheric Transport of Air Pollution version 3 (HTAPv3) inventory (Crippa et al., 2023), using the 2018 base year, regridded to the model's T106 horizontal resolution. Agricultural sector emissions are excluded from HTAPv3 to avoid double-counting with agricultural fires in GFASv1.2. Biogenic isoprene emissions are from the Model of Emissions of Gases and Aerosols from Nature version 2 (MEGANv2) (Guenther et al., 2012). Soil NO_x emissions are prescribed from the Global Emissions Inventory Activity (GEIA) (Graedel et al., 1993).

The assimilated data are the v4.3 profile retrievals of O_3, CO, and HNO_3 from the Microwave Limb Sounder (MLS) (Livesey et al., 2008; Santee et al., 2007), v9 MOPITT CO column measurements (Deeter et al., 2017), tropospheric NO_2 columns (van Geffen et al., 2022), total SO_2 columns (Theys et al., 2021), and tropospheric CH_2O columns from TROPOMI (De Smedt et al., 2021). We also assimilate VIIRS AOD products from the Deep Blue Aerosol L2 6-min Swath 6 km version 2 (AERDB_L2_VIIRS_SNPP and AERDB_L2_VIIRS_NOAA20) products. To reduce computational cost and minimize representation errors in the data assimilation calculations, the super-observation approach is applied to the high-resolution TROPOMI NO_2, SO_2, and CH_2O data (Rijsdijk et al., 2025). The observation operator is constructed based on the prior profiles and averaging kernels of the assimilated retrievals. To evaluate the impact of data assimilation, we also analyze the control (CTL) simulation, which is performed without assimilation.

We conduct an additional sensitivity experiment for CO, in which Community Emissions Data System version v2021-04-21 (CEDS) (Hoesly et al., 2018) and Global Fire Emission Database version 4 (GFED4) (Giglio et al., 2013) are used as the prior anthropogenic and biomass burning emission inventory, respectively, and TROPOMI CO column measurements (Borsdorff et al., 2018) are assimilated in place of MOPITT CO. The results are discussed alongside the standard TCR-3 evaluation in Sections 3 and 4.

https://doi.org/10.5194/egusphere-2026-2380
Preprint. Discussion started: 8 May 2026

2.2 ASIA-AQ DC-8 airborne observations

ASIA-AQ is a multinational field campaign led by NASA in collaboration with international partners in the Philippines, Taiwan, South Korea, and Thailand. Conducted in February and March 2024, the mission integrated airborne sampling, satellite retrievals, and ground-based monitoring to investigate emission sources, atmospheric chemistry processes, and transboundary transport mechanisms across Northeast and Southeast Asia. ASIA-AQ was designed to address several key objectives, including validation of satellite retrievals, particularly from GEMS, quantification and verification of emissions from key source regions, evaluation of chemical transport models, and characterization of aerosol and O_3 chemistry.

The campaign deployed the NASA DC-8 aircraft for 16 research flights across the four participating regions between February 6 and March 27, 2024 (Figure 1). The aircraft measured over 100 trace gases and aerosol properties. For comparing with the TCR-3 reanalysis, this study focuses on measurements of O_3, NO_x, CO, and CH_2O. Figure 2 illustrates the time–altitude distributions of these species, alongside isoprene, highlighting the diverse pollution regimes sampled during the campaign, including urban emissions, biomass burning plumes, and biogenic-influenced air masses.

Table 1. DC-8 observation data from NASA's ASIA-AQ campaign used for model evaluation. Data are from the 1-minute merged dataset downloaded on April 14, 2024.

Species	Instrument	Uncertainty	Institution	Reference
O_3	Chemiluminescence instrument (NOxO3)	2-sigma accuracy of 5%*	National Center for Atmospheric Research (NCAR)	Ridley et al., 1992
	Rapid Ozone Experiment (ROZE)	1-sigma accuracy of 6.2%	NASA Goddard Space Flight Center	Hannun et al., 2020
NO_x	Chemiluminescence instrument (NOxO3)	2-sigma accuracy of 8% for NO and 11% for NO_2	National Center for Atmospheric Research	Ridley et al., 1992
CO	Diode Laser Spectrometer (DACOM)	uncertainty of 2% (<1 ppm) to 5% (>1 ppm)	NASA Langley Research Center	Diskin et al., 2002
	Quantum Cascade Laser Absorption Spectrometer (MIRO)	the mean precision of 0.15 ppbv and the mean relative total uncertainty that can be up to 10%	Deutsches Zentrum für Luft- und Raumfahrt (DLR)	Knez et al., 2026
CH_2O	In Situ Airborne Formaldehyde instrument (ISAF)	accuracy of 10% + 10 pptv	NASA Goddard Space Flight Center	Cazorla et al., 2015
	Trace Organic Gas Analyzer with Time-of-Flight Mass Spectrometer (TOGA-TOF)	uncertainty of 35% and a lower limit of detection of 20 pptv	NSF NCAR Atmospheric Chemistry Observations & Modeling Laboratory	Jeong et al., 2025
Isoprene	Whole Air grab Samples analyzed via gas chromatography and mass spectrometry (WAS)	Precision of 3% and accuracy of 5% (Simpson et al., 2010)	University of California Irvine	Simpson et al., 2020

https://doi.org/10.5194/egusphere-2026-2380
Preprint. Discussion started: 8 May 2026

* The data additionally account for the uncertainty due to the unknown influence of water vapor inside the reaction vessel. Total uncertainties are provided as dependent variables in the data file and are shown as additional error bars in the vertical distributions in Fig. 5 (Section 3).

To facilitate direct comparison with the two-hourly TCR-3 reanalysis data, the 1-minute averaged observational data in Table 1 are further averaged into the two-hour windows and regridded to match the model's horizontal and vertical resolution. Additionally, we employ smoke and combustion classification flags developed by Miech et al. (2025) to qualitatively identify biomass burning influences. The campaign sampled distinct meteorological conditions and emission regimes across the four domains (Fig. 2). In the Philippines, the first two flights occurred during weak Northeast Monsoon conditions, while the latter two flights sampled during a strengthened Northeast Monsoon. Taiwan flights captured contrasting meteorological regimes, with the first flight conducted in pre-frontal conditions and the latter two in post-frontal environments. Thailand experienced weak synoptic flow during the first two flights, with the most severe pollution burdens observed as elevated concentrations of CO coincided with extensive biomass burning activity. A precipitation event on March 20 preceded the third Thailand flight on March 21, resulting in notably cleaner atmospheric conditions. Overall, meteorological conditions during the campaign were largely consistent with climatological norms for this season (Fig. S1). February was defined by a robust winter monsoon circulation driving northwesterly flow over Northeast Asia, while March marked a seasonal transition toward spring, characterized by weakened circulation and enhanced convection over the Maritime Continent.

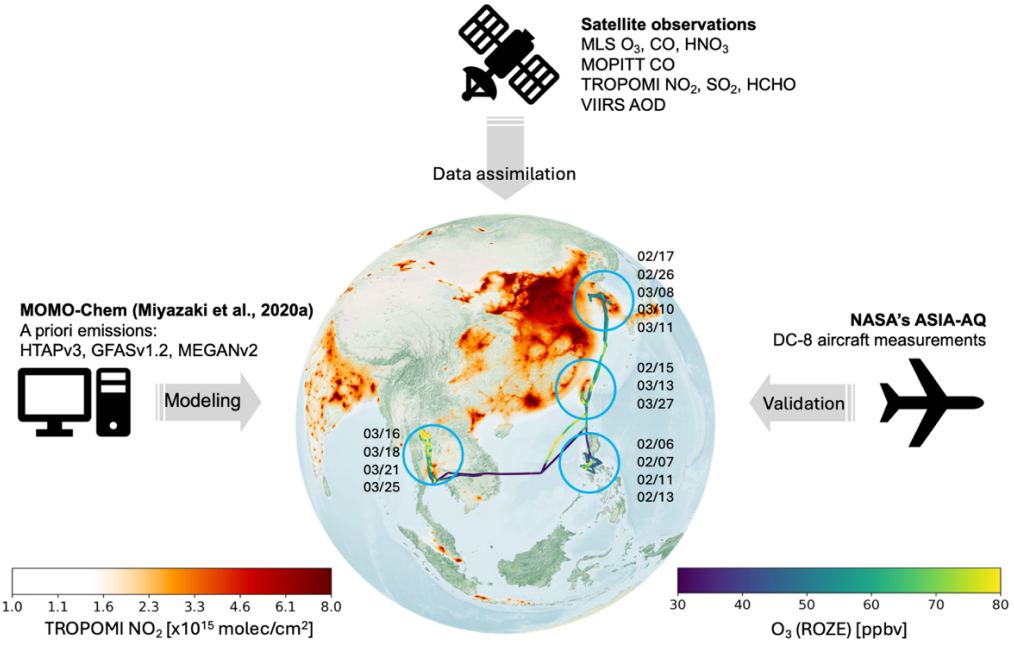

Figure 1. Schematic diagram of MOMO-Chem data assimilation framework integrating global multi-constituent satellite observations. The globe displays the 2024 annual mean TROPOMI NO_2 column densities, with four blue circles highlighting the four ASIA-AQ study regions: the Philippines, Taiwan, South Korea, and Thailand. The DC-8 flight tracks are overlaid on

https://doi.org/10.5194/egusphere-2026-2380
Preprint. Discussion started: 8 May 2026

the globe and are color-coded by O_3 (ROZE) mixing ratios across all altitudes. Flight dates are labelled adjacent to each study region.

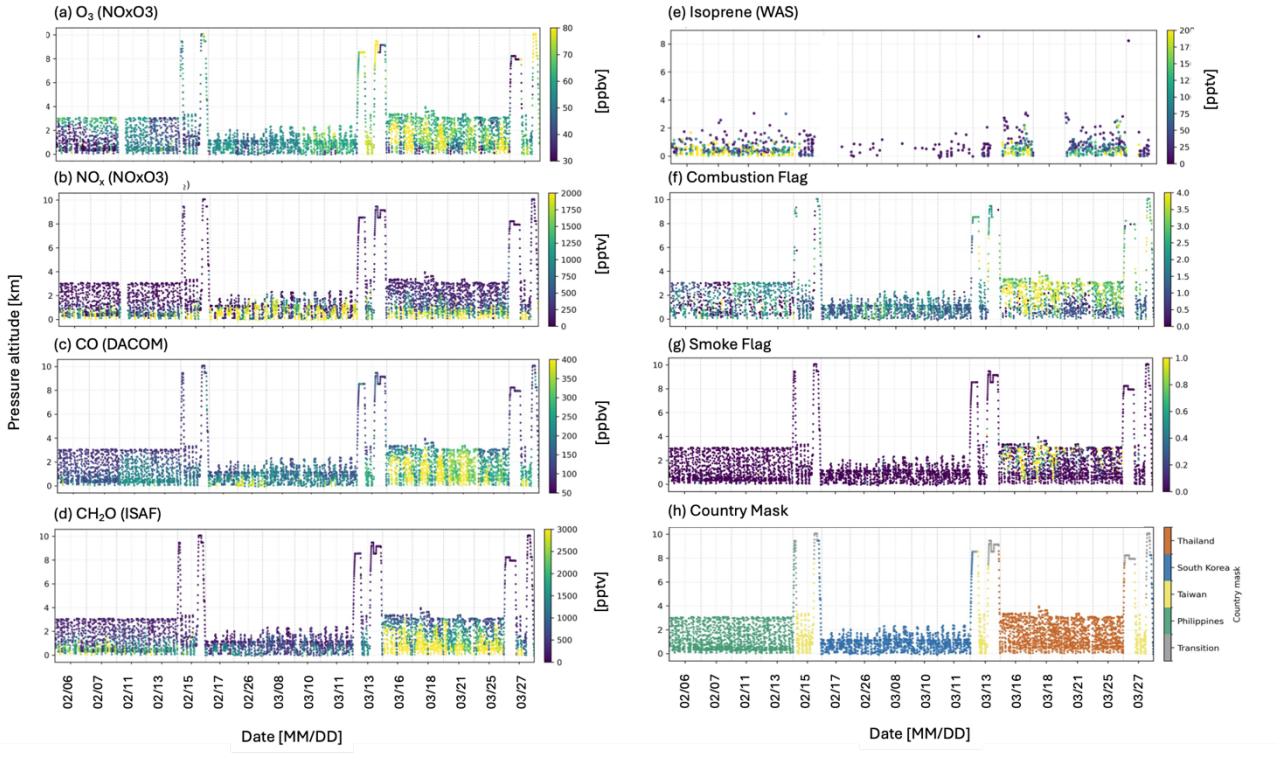

Figure 2. Time–altitude distributions of 1-min-averaged (a) O_3 from NOxO3, (b) NO_x from NOxO3, (c) CO from DACOM, (d) CH_2O from ISAF, and (e) isoprene from WAS aboard the DC-8 during ASIA-AQ, colored by observed mixing ratios. Panels (f) and (g) show the combustion and smoke flags, and panel (h) indicates the regional mask used to classify flight segments over the Philippines, Taiwan, South Korea, Thailand, and transition regions. The combustion flag (1 = higher combustion efficiency, 2 = mid, 3 = low, 4 = lowest) represents combustion characteristics inferred from CO/CO_2 enhancement ratios and can be associated with biomass-burning conditions. The smoke flag identifies the influence of biomass burning (0 = lack of clearly defined biomass burning influence, 1 = clearly influenced).

3 Evaluation of TCR-3 against DC-8 measurements

We evaluate the TCR-3 chemical reanalysis against the DC-8 measurements of O_3, NO_x, CO, and CH_2O. Reanalysis-measurement agreement is assessed using near-surface (below 1 km) spatial distributions (Fig. 3), time series along the flight tracks (Fig. 4), and vertical profiles (Fig. 5). Aggregate statistics for the entire campaign dataset are summarized in Table 2.

https://doi.org/10.5194/egusphere-2026-2380
Preprint. Discussion started: 8 May 2026

Table 2. Summary statistics of the control simulation (CTL, without DA) and TCR-3 (with DA) evaluated against the DC-8 observations for the entire ASIA-AQ campaign. Observations are matched to their corresponding model grid cells in horizontal and vertical space and averaged within two-hour windows. Statistics are computed across all matched observation-model pairs spanning the full range of flight altitudes. R = correlation coefficient; NMB = Normalized Mean Bias (%); RMSE = Root Mean Square Error (ppbv).

Species	Instrument	Simulation	R	NMB (%)	RMSE (ppbv)
O_3	NOxO3	CTL	0.50	−17.4	17.1
		TCR-3	0.59	−13.9	15.3
	ROZE	CTL	0.47	7.31	12.5
		TCR-3	0.58	11.9	12.6
NO_x	NOxO3	CTL	0.72	−14.7	2.60
		TCR-3	0.66	−29.7	2.62
CO	DACOM	CTL	0.64	−32.1	107
		TCR-3 (MOPITT)	0.77	−15.4	76.5
		TCR-3 (TROPOMI)	0.77	−0.5	87.5
	MIRO	CTL	0.60	−32.4	114
		TCR-3 (MOPITT)	0.75	−15.6	80.4
		TCR-3 (TROPOMI)	0.77	1.0	90.3
CH_2O	ISAF	CTL	0.75	54.6	1.78
		TCR-3	0.77	16.6	1.14
	TOGA-TOF	CTL	0.77	70.1	1.77
		TCR-3	0.79	29.4	1.16

3.1 CO

Observed CO shows pronounced regional variability, with highest concentrations over Thailand (mean ~310–316 ppbv, reaching 1,048 ppbv during biomass burning episodes), followed by Taiwan (~199–206 ppbv), South Korea (~195 ppbv), and the Philippines (~153–155 ppbv). They exhibit gradual decreases with altitude, with concentrations declining from peak boundary layer values to ~100–200 ppbv at 3–4 km. The surface elevated layers extend to 2–3 km over Thailand. TCR-3 shows substantial improvements for CO across all regions. The control simulation (CTL) exhibits a consistent low bias throughout the domain, with a Normalized Mean Bias (NMB) of −32.1% and −32.4% against DACOM and MIRO CO, respectively (Table 2). TCR-3 reduces the NMB to −15.4% and −15.6% while increasing the correlation coefficient (R) from 0.60–0.64 to 0.75–0.77 domain-wide. Particularly significant improvements occur over Thailand, where the correlation strengthens markedly (from 0.07 to 0.50 below 1 km against DACOM) and CTL substantially underestimates elevated CO.

https://doi.org/10.5194/egusphere-2026-2380
Preprint. Discussion started: 8 May 2026

TCR-3 better captures the observed high surface peaks in Northern Thailand exceeding 800 ppbv (Fig. 3), as well as their temporal variability during episodic burning events in March (Fig. 4), reducing the surface NMB from −28% to −8%. Modest improvements are also evident over the Philippines (where R increases from 0.48 to 0.62 and NMB improves from −35% to −22% below 1 km) and Taiwan (R increases from 0.76 to 0.81), while improvements are less pronounced over South Korea.

TROPOMI TCR-3, the additional sensitivity experiment described in Section 2.1, yields a near-zero NMB (−0.5% and +1.0% against DACOM and MIRO, respectively) compared to −15.4% and −15.6% in the standard MOPITT TCR-3, with comparable R (0.77) but higher RMSE (88–90 ppbv vs. 77–80 ppbv) (Table 2). Notably, TROPOMI TCR-3 reduces the underestimation of elevated CO at ~2 km altitude over Thailand (NMB of ~+3 to +4% above 2 km compared to ~−18% in the standard TCR-3). This improvement is associated with increased CO emissions in Northwest Thailand and Myanmar constrained by TROPOMI (Section 4), which alters the spatial distribution of biomass burning emissions and their subsequent transport aloft. However, TROPOMI TCR-3 simultaneously overestimates the DC-8 near-surface concentrations, with mean values reaching ~449 ppbv against observed ~337–345 ppbv (~30% overestimation) compared to ~318 ppbv in the standard TCR-3 (Fig. 5). This trade-off (better free-tropospheric performance at the cost of surface overestimation) is particularly evident in Northern Thailand, and may suggest that the model places too large a fraction of these emissions near the surface, or that vertical mixing in the model does not efficiently redistribute them aloft. This also points to uncertainties in the vertical distribution of biomass burning emissions, particularly their injection heights, as a key limiting factor in reproducing the observed vertical CO profile (Pan et al., 2026).

3.2 CH_2O

Observed CH_2O concentrations show strong regional gradients, with the highest values over Thailand (mean 2.3–2.6 ppbv, ranging up to 14.9 ppbv), followed by the Philippines (1.0–1.4 ppbv), Taiwan (1.0–1.2 pp), and South Korea (~0.6 ppbv). CH_2O decreases with altitude more steeply than CO due to its shorter atmospheric lifetime, yielding strong vertical gradients below 2 km (Fig. 5) that reflect surface emissions and secondary production from VOC oxidation near the surface. CTL overestimates the boundary layer (below 1 km) CH_2O across the domain, with NMBs of +89% and +85% against ISAF and TOGA-TOF. When aggregated over all altitudes, CTL shows domain-wide NMB of +54.6% against ISAF and +70.1% against TOGA-TOF (Table 2). Data assimilation reduces these biases to +16.6% and +29.4%, respectively, consistent with decreased isoprene emissions (Section 4), with greater improvements over the Philippines (surface NMB reduced from +74% to +22%) and Thailand (surface NMB reduced from +87% to +43%). Over Taiwan, surface NMB decreases from +109% to +48%. Above 2 km over Thailand, the CTL positive bias decreases from +27% to +7% in TCR-3, while the correlation increases from 0.58 to 0.64.

https://doi.org/10.5194/egusphere-2026-2380
Preprint. Discussion started: 8 May 2026

3.3 O_3

Observed O_3 concentrations range from 38–48 ppbv over the Philippines to 52–57 ppbv over South Korea and Taiwan, and 51–66 ppbv over Thailand. O_3 generally increases with altitude over the Philippines and South Korea (Fig. 5), but decreases over Taiwan. The highest O_3 occurs during biomass burning episodes over Thailand, where concentrations exceed 127 ppbv. Validation of O_3 is complicated by substantial differences between the two measurement instruments. Against NOxO3, CTL shows NMB of −17.4% and R of 0.50, while TCR-3 reduces the bias to −13.9% and improves R to 0.59 (Table 2). Relative to ROZE, the positive bias increases from +7.3% in CTL to +11.9% in TCR-3, although R still improves from 0.47 to 0.58. Except over the Philippines, the assimilation generally increases O_3 throughout the troposphere. In the lower troposphere at low latitudes, these adjustments are primarily driven by precursor emission optimization, while assimilation of MLS O_3 in the UTLS exerts a large influence in the extratropic (Miyazaki et al., 2020; Selina et al., 2025). Thailand shows the most substantial improvements. Below 1 km, R increases from 0.39 to 0.67 against NOxO3 and from 0.42 to 0.66 against ROZE. Above 2 km, R improves from 0.26 to 0.61 against both instruments, with NMB improving from −24% to −13%. Episodic enhancements associated with biomass burning plumes over Thailand in late March are better captured by TCR-3, though peak concentrations remain slightly underestimated (Fig. 4). Over South Korea, Taiwan, and the Philippines, R increased by 0.05–0.10 in the boundary layer.

3.4 NO_x

South Korea shows the highest surface NO_x associated with urban and industrial emissions, followed by Thailand, Taiwan, and the Philippines. Although the overall benefit of assimilation is not evident when evaluated against NOxO3 measurements aggregated over all altitudes (Table 2), the impact varies substantially by region and altitude. In Taiwan, assimilation reduces the negative bias, improving NMB from −55% to −45% below 1 km and from −62% to −50% above 2 km. In the Philippines above 2 km, NMB improves from −53% to −27%, though R decreases from 0.62 to 0.30. Over South Korea below 1 km, CTL shows a slight positive bias (+25% NMB) that shifts to a negative bias of −18% in TCR-3. Over Thailand, assimilation increases the negative bias from −36% to −43% below 1 km, while reducing the larger negative biases from −65% to −44% and increasing R from 0.11 to 0.48 above 2 km. Underestimation of boundary layer NO_x has been commonly reported by previous studies (Miyazaki et al., 2012; Skoulidou et al., 2021). Increasing model resolution remains essential to resolve urban plumes and their non-linear chemistry (Valin et al., 2011; Sekiya et al., 2021). Evaluation against NO_2 measurements from NOxO3 shows a similar pattern (not shown). CTL shows a near-neutral domain-wide bias (+2% NMB) with R of 0.68, while TCR-3 introduces a negative bias (−19% NMB) with R reducing to 0.62, consistent with the NO_x results. In contrast to NO_x, whose RMSE increases slightly with assimilation (Table 2), RMSE for NO_2 improves from 3.0 to 2.6 ppbv.

https://doi.org/10.5194/egusphere-2026-2380
Preprint. Discussion started: 8 May 2026

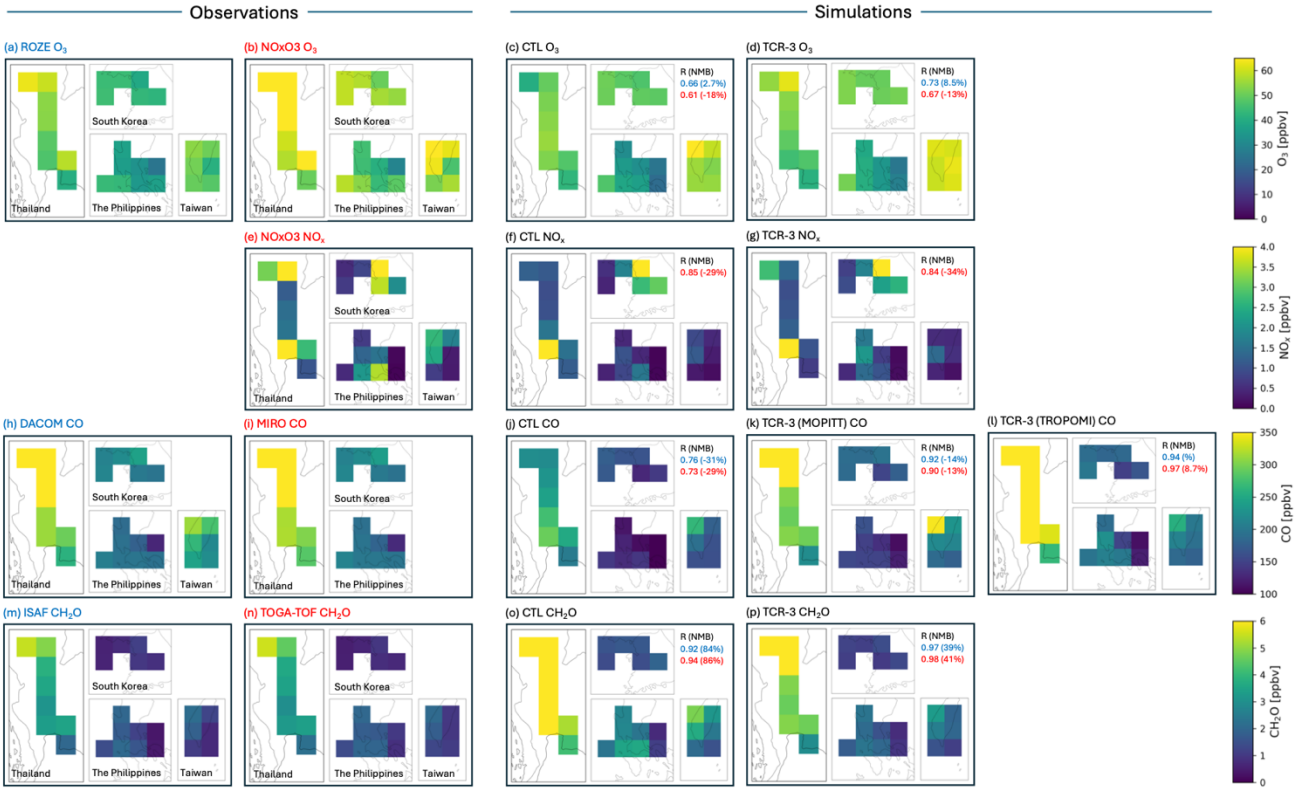

Figure 3. Spatial distributions of near-surface concentrations (below 1 km) during ASIA-AQ on the TCR-3 grid at 1.125° × 1.125°. Panels are organized by species and dataset. For O_3, panels (a) ROZE and (b) NOxO3 show observations, followed by simulations in (c) CTL and (d) TCR-3. For NO_x ($NO + NO_2$), panel (e) NOxO3 shows observations, followed by (f) CTL and (g) TCR-3. For CO, panels (h) DACOM and (i) MIRO show observations, followed by (j) CTL, (k) TCR-3 constrained with MOPITT, and (l) TCR-3 constrained with TROPOMI. For CH_2O, panels (m) ISAF and (n) TOGA-TOF show observations, followed by (o) CTL and (p) TCR-3. Correlation coefficient R and normalized mean bias NMB are calculated for each simulation against the corresponding observations; when two observational datasets are available, statistics relative to the first observation are shown in blue and those relative to the second observation are shown in red. For the spatial distribution analysis of CO in Taiwan, only DACOM observations were used.

https://doi.org/10.5194/egusphere-2026-2380
Preprint. Discussion started: 8 May 2026

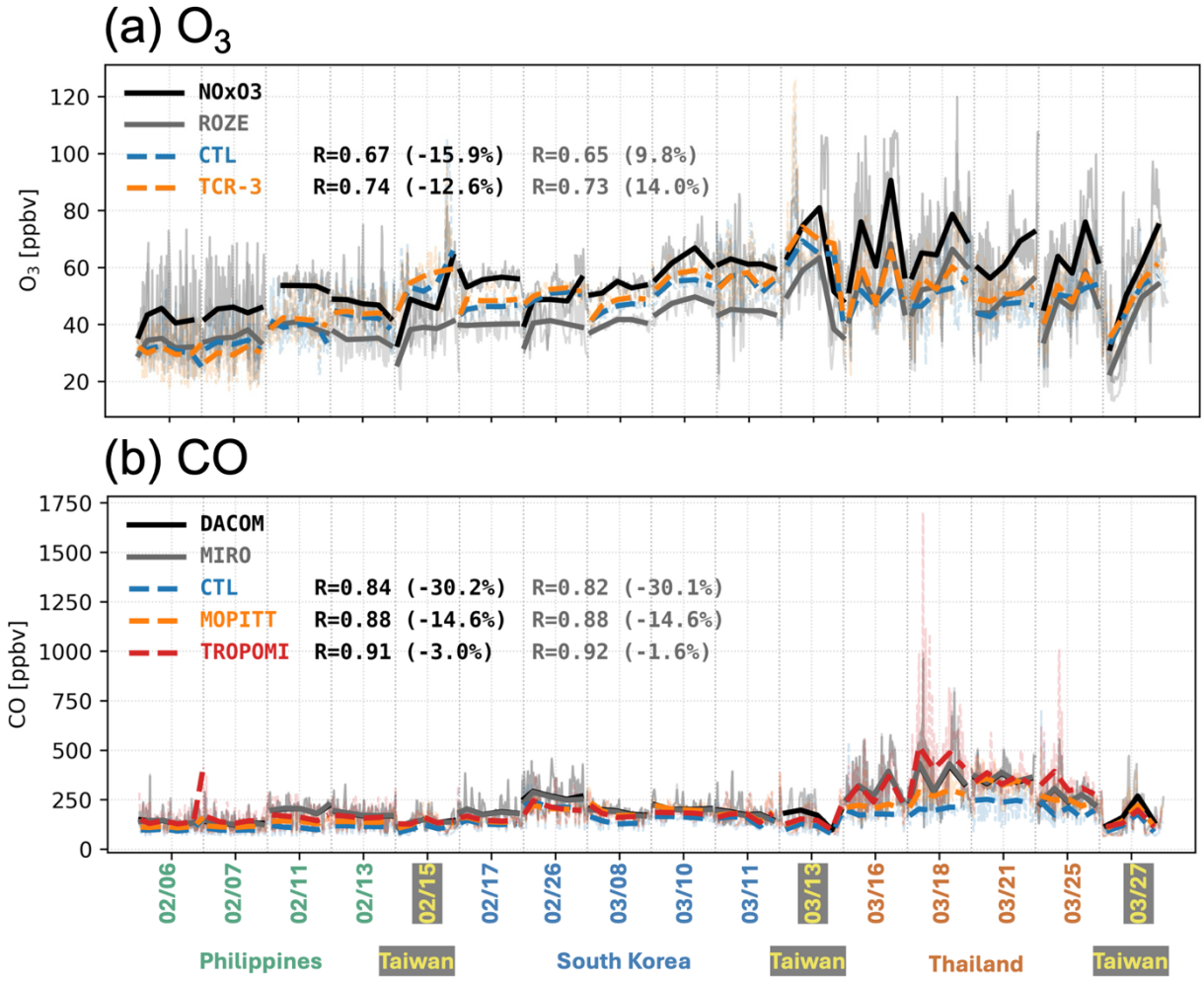

Figure 4. Temporal evolution of (a) O_3 and (b) CO during ASIA-AQ DC-8 flights (February–March 2024) shown in sequential-ordinal representation. Thick lines show two-hour temporal averages for observations (NOxO3/ROZE for O_3; DACOM/MIRO for CO) and model simulations (CTL and TCR-3 for O_3; CTL and TCR-3 constrained by MOPITT and TROPOMI for CO). Thin background lines show observations and model output regridded to model horizontal and temporal (two-hourly) resolution along the flight track, illustrating spatial variability within each two-hour period. Data are plotted as a discontinuous timeseries, preserving the sampling order within each day while including visual breaks between dates to reflect the non-continuous observations. Correlation coefficients (R) and normalized mean bias (NMB%) are calculated from the two-hourly averaged data. Grey vertical lines denote calendar date boundaries.

https://doi.org/10.5194/egusphere-2026-2380
Preprint. Discussion started: 8 May 2026

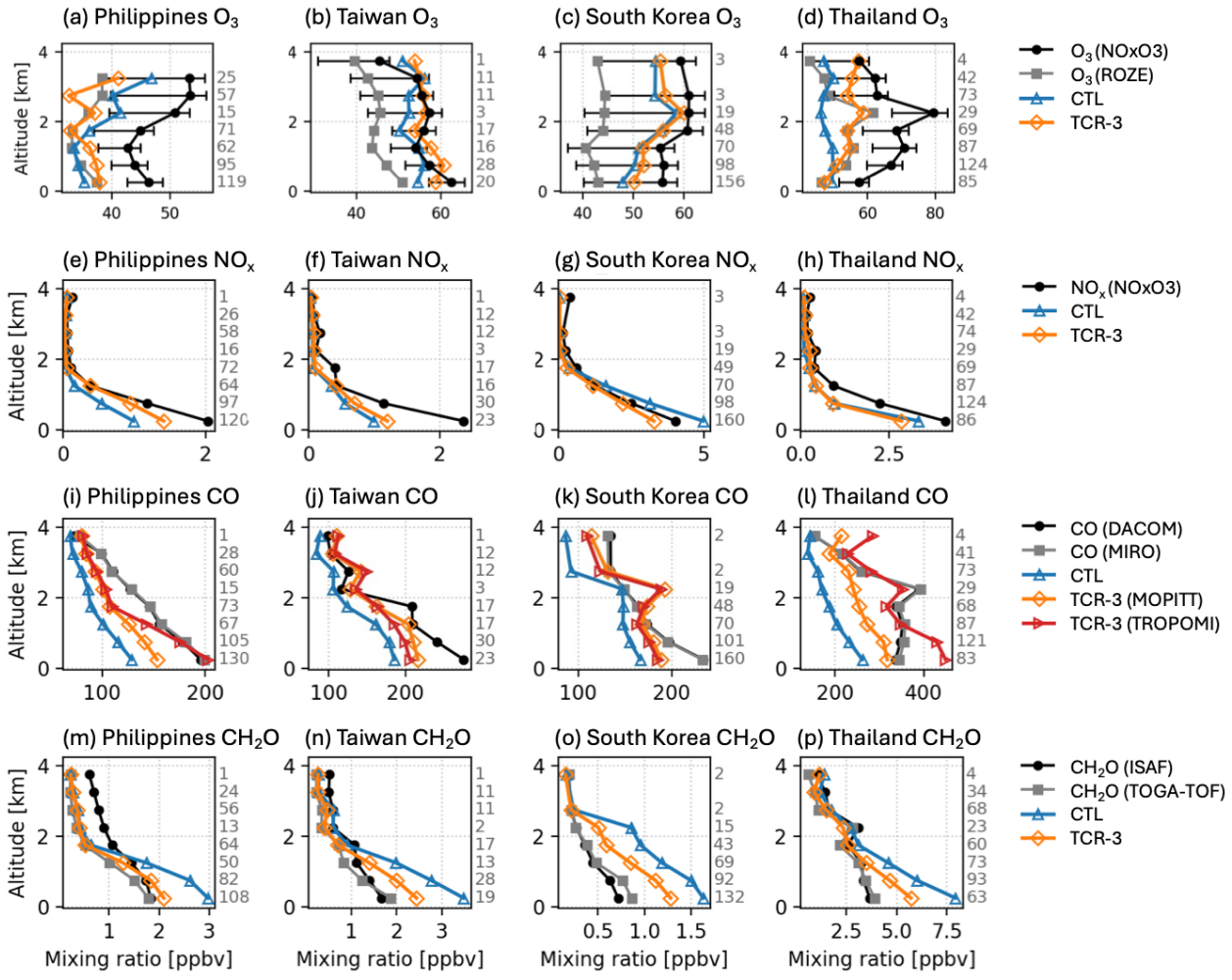

Figure 5. Vertical profiles of O_3 (a–d), NO_x (e–h), CO (i–l), and CH_2O (m–p) over four ASIA-AQ regions: the Philippines (a, e, i, m), Taiwan (b, f, j, n), South Korea (c, g, k, o), and Thailand (d, h, l, p). Black and grey curves with filled markers represent 1-min-averaged DC-8 observations, the blue curves with open triangles indicate the CTL simulation, and the orange curves with open diamonds show the TCR-3 posterior simulation. Specifically for the CO panels, the red curves with open right-pointing triangles show the TCR-3 (TROPOMI) posterior simulation. Numbers on the right y-axes indicating the number of data points. For O_3, additional error bars on the black curves represent the total uncertainty of the NOxO3 instrument, accounting for the unknown influence of water vapor inside the reaction vessel. For the vertical distribution analysis of CO in Taiwan, only DACOM observations were used.

https://doi.org/10.5194/egusphere-2026-2380
Preprint. Discussion started: 8 May 2026

4 Estimated NO_x, CO, and Isoprene emissions

Figure 6 shows the optimized total emissions from TCR-3 and their adjustments relative to the prior emissions for NO_x, CO, and isoprene during February–March 2024. We primarily focus on O_3 and its precursors in this analysis. The regional total NO_x emissions increase by 15% in TCR-3 relative to the prior, reflecting increases across continental Southeast Asia (+39%) in contrast to decreases in mainland China (−9%). At the national scale, the largest relative increases are found in Myanmar (+143%), Laos (+115%), and Cambodia (+95%). Among the four ASIA-AQ flight regions, South Korea shows a broad decrease (-18%). Taiwan (+14%), Thailand (+18%), and the Philippines (+36%) show spatially heterogeneous adjustments, with reductions over major urban areas (e.g., southwest Taiwan, Bangkok, southern Manila, Cebu) and increases elsewhere modulating the urban-rural gradients. Over East Asia, total ship NOx emissions also increase by approximately 59 %.

The regional total CO emissions increase by 9%, reflecting increases in continental Southeast Asia (+33%). Over China, assimilation decreases CO emissions by 18% in the eastern industrial corridor (28–42°N, 110–122°E; from 13.2 to 11.4 Tg) and increases them by 27% in southwestern China near the Myanmar/Laos border (21–30°N, 97–108°E; from 2.3 to 4.3 Tg), collocated with biomass burning areas. Increases exceeding +100 % are found in Laos and Cambodia. Unlike NO_x, CO emissions increase over South Korea (+34%). Taiwan shows similar increases (+25%), whereas Philippines shows decreases (−41%). Thailand exhibits large increases (+52%), driven primarily by enhanced emissions outside Bangkok in regions impacted by biomass burning.

Isoprene emissions decrease by 52% domain-wide, with pronounced reductions across Maritime Southeast Asia (−70%), the Philippines (−63%), Taiwan (−71%), Thailand (−40%), and South Korea (−69%). These reductions are consistent with previous studies showing MEGAN overestimates isoprene emissions over Southeast Asian tropical forests by factors of 2-4 (Langford et al., 2010; Stavrakou et al., 2014). In contrast, mainland China shows an increase (+60%). The adjustments underscore the substantial uncertainties in bottom-up isoprene inventories over Asian tropical regions, with important implications for O_3 production, OH budgets, and secondary organic aerosol formation (Yoon et al., 2025). At the same time, the top-down isoprene estimates remain subject to considerable uncertainty. They are sensitive to the representation of isoprene chemistry and the broader chemical environment within the model (Choi et al., 2025; Wells et al., 2020; Yang et al., 2023). In addition, potential biases in the assimilated TROPOMI CH_2O retrievals may influence the optimized emissions and require further investigation (Oomen et al., 2024).

https://doi.org/10.5194/egusphere-2026-2380
Preprint. Discussion started: 8 May 2026

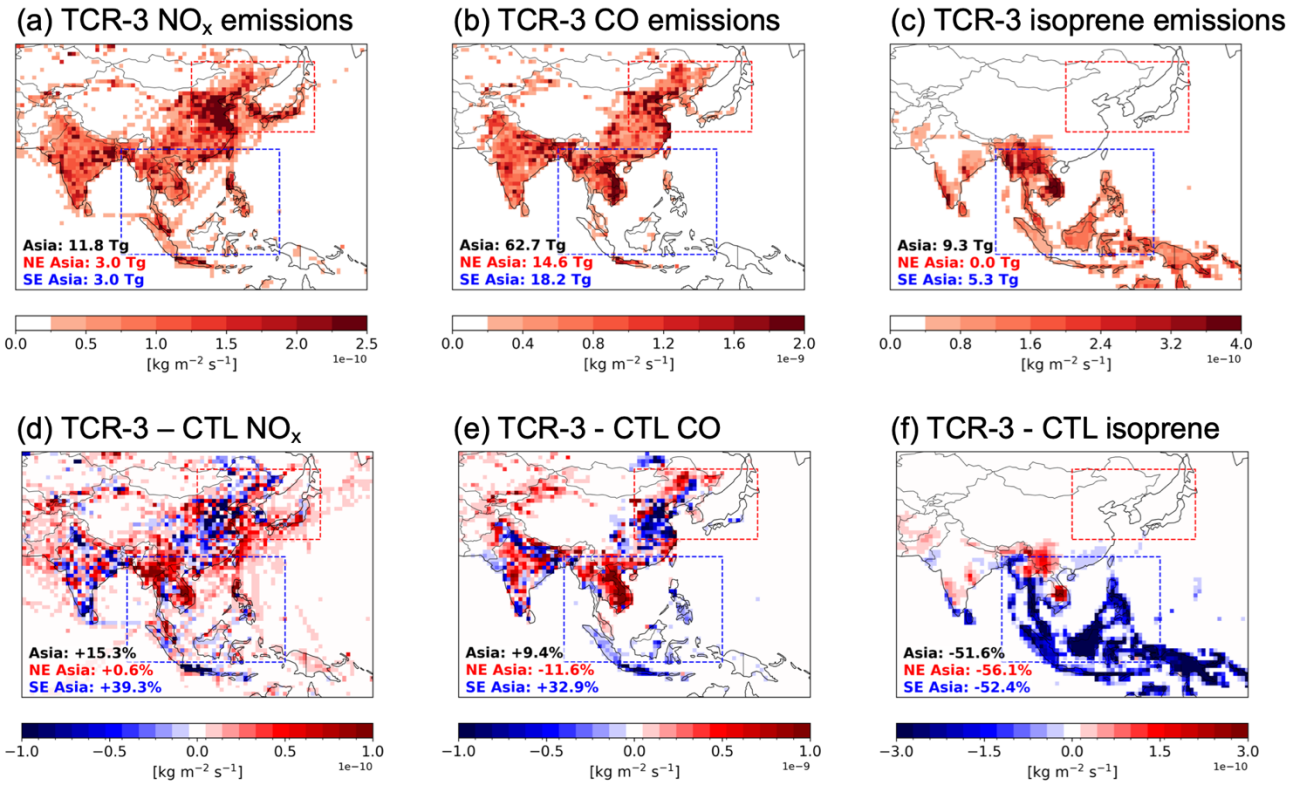

Figure 6. Spatial distributions of NO_x (left), CO (center), and isoprene emissions (right) averaged over February–March 2024 from the TCR-3 (upper panels) and their differences relative to the prior emissions (lower panels). Domain-total emissions are indicated in teragrams (Tg) in panels (a–c), and percentage changes relative to the prior emissions are shown in panels (d–f).

4.1 Anthropogenic emissions

We compare our top-down estimates with five bottom-up inventories: HTAPv3 and HTAPv3.2 (Crippa et al., 2023; Guizzardi et al., 2025), Air Quality North East Asia version 4 (AQNEAv4), the Emissions Database for Global Atmospheric Research version 8.1 (EDGARv8.1, https://edgar.jrc.ec.europa.eu/dataset_ap81, Crippa et al., 2020), CEDSv2025-04-18 (Hoesly et al., 2018), and the Copernicus Atmosphere Monitoring Service Global Anthropogenic Emissions version 6.2 (CAMS-GLOB-ANTv6.2) and mosaic version 1.0 (CAMS-GLOB-ANTm1.0) (https://permalink.aeris-data.fr/CAMS-GLOB-ANT, Denier van der Gon et al., 2025; Soulie et al., 2024). For this comparison, the top-down total emissions at each grid cell are partitioned into anthropogenic, biomass-burning, and biogenic components using the a priori fractional contributions from each sector

https://doi.org/10.5194/egusphere-2026-2380
Preprint. Discussion started: 8 May 2026

(see Section 2.1). The resulting TCR-3 sectoral emissions are then downscaled to 0.1° × 0.1° resolution using spatial proxies derived from the a priori emissions. Ship emissions are not included in the region-specific analysis. Regional totals (anthropogenic + biomass burning) of TCR-3 NOx and CO emissions for February-March 2024 are summarized in Table S1.

EDGARv8.1 provides globally consistent emissions for the 1970–2022 period by applying standardized methodologies and default emission factors across all countries. EDGAR serves as a foundational baseline for several other inventories compared in this study (HTAP, CEDS, and CAMS-ALOG-ANT) and therefore these inventories are not fully independent of each other. HTAPv3 covers 2000-2018 using EDGARv6.1 as a baseline, integrated with regional data such as REASv3.2.1 for East and Southeast Asia (Kurokawa and Ohara, 2020). HTAPv3.2 extends this coverage to 2020, updates the baseline to EDGARv8, and incorporates MEICv1.4 for China (Wu et al., 2024). AQNEAv4, developed by Seoul National University for the ASIA-AQ campaign, integrates 2019 national data for East Asia with local datasets for Taiwan (base year 2024) and Thailand (base year 2022), alongside MIXv2.3 (Li et al., 2024) for background regions. CEDSv2025-04-18 covers 1980-2023. CAMS-GLOB-ANTv6.2, part of the Copernicus Atmosphere Monitoring Service (CAMS), covers 2000-2025. We use CAMS-GLOB-ANTm1.0 for 2024, which utilizes MEICv1.4 for China (Wu et al., 2024). Sectoral contributions are further examined using the IPCC 2006 categories: Power (1A1), Industry (1A2, 1B, 2), Residential + Commercial + Others (Buildings; 1A4, 1A5), Transport (1A3), and Agriculture (3A, 3C, 5A, 4).

Figures 7 and 8 present time series of average February–March anthropogenic NO_x and CO emissions for 2000–2025, placing the 2024 TCR-3 estimates in the context of historical inventory trends. The spread among inventories is wider for CO than NO_x, likely reflecting the stronger sensitivity of CO emissions to combustion conditions, technology types, and emission factor assumptions. Figure 9 provides a detailed sectoral breakdown for each inventory using the closest year to the 2024 ASIA-AQ period. For NO_x, transport is the dominant sector across most regions and inventories, with exceptions in mainland China and India, where industry and power lead, respectively, in several datasets. For CO, the dominant sector varies more widely by region and inventory. Among these inventories, CEDS attributes a larger fraction of national CO totals to the power sector (8–48%) compared to other inventories (1–7%, except AQNEAv4 in South Korea at 12%), accompanied by comparatively small industry sector contributions. EDGAR shows lower transport contributions for both CO and NOx across most regions, with CO transport fractions of only 3–4% in mainland China, India, and the Philippines compared to 6–19%, 11–26%, and 20–35%, respectively, in other datasets.

Following the approach of Crippa et al. (2023) and Guizzardi et al. (2025), we quantify the range of estimates by calculating the coefficient of variation (CV; standard deviation divided by mean) across five inventories with the same base year (2019). Figures 10 and S2 show the spatial distribution of inter-inventory CV at 0.1° × 0.1° resolution by sector for NO_x and CO, respectively. Figure S3 provides the CV aggregated by region for both NO_x and CO. Across sectors, the power sector exhibits the largest inter-inventory variability, with CVs exceeding 120% over most regions and surpassing 200% in parts of India. The

https://doi.org/10.5194/egusphere-2026-2380
Preprint. Discussion started: 8 May 2026

industry sector also shows substantial variability, with CVs typically in the range of 90-120%. In contrast, the buildings sector has lower variability, although moderate CVs are evident in several ASIA-AQ study regions, including Thailand, South Korea, and the Philippines. Transport displays a more spatially heterogeneous pattern, with higher CVs occurring outside major transport corridors, indicating greater disagreement in the representation of diffuse and non-highway emission sources (Fig. S4).

The intercomparison of emissions is discussed separately for each region below.

Mainland China

Inventories consistently show declining NO_x and CO emissions after 2012 (Fig. 7, 8). For NO_x, trends before 2020 are comparable across HTAP, EDGAR, and CEDS (−92 to −115 Gg month^{-1} yr^{-1}), while CAMS-GLOB-ANT shows a substantially weaker decline (−27 Gg month^{-1} yr^{-1}). This discrepancy is primarily driven by the power sector, which exhibits a much smaller decreasing trend in CAMS-GLOB-ANT. Inter-inventory agreement is relatively strong in 2019 (CV = 11%; Fig. S3). Beginning in 2021, EDGAR and CEDS indicate increasing NO_x emissions, whereas CAMS-GLOB-ANT shows a rebound in 2021 followed by a renewed decline. Among regional inventories, AQNEA (2019) yields the lowest estimates, while CAMS-GLOB-ANTm1.0, which incorporates MEICv1.4 for China, produces higher emissions than CAMS-GLOB-ANTv6.2. TCR-3 estimates for 2024 fall at the upper end of the inventory range.

For CO, emission reductions between 2012 and 2020 are larger in magnitude (−192 to −898 Gg month^{-1} yr^{-1}) than after that period, with CAMS-GLOB-ANT again showing the slowest decline. These reductions are mainly driven by the industry and buildings sectors. Although inter-inventory spread is substantial in the early 2000s, it narrows over time, reaching a CV of 19% by 2019. AQNEA (2019) provides the highest CO estimates among inventories, and both TCR-3 products exceed CAMS-GLOB-ANT inventories in 2024.

Transport exhibits large inter-inventory variability outside major highway corridors for both NO_x and CO (Figs. 10, S2, S4). This likely reflects the limited representation of area sources in global inventories compared to HTAP and AQNEA, suggesting a potential underestimation of emissions from secondary roads and non-road machinery.

India

All inventories show increasing NO_x emissions prior to 2020 (21–32 Gg month^{-1} yr^{-1} since 2000), largely driven by the power sector, with moderate inter-inventory agreement in 2019 (CV = 11%). HTAP reports higher NO_x emissions than other inventories, potentially reflecting different assumptions regarding the penetration of low-NO_x burner technologies. TCR-3 follows the general increasing trajectory, similar to CAMS-GLOB-ANT, and lies between lower estimates (AQNEA, EDGAR, CEDS) and higher estimates (HTAP).

https://doi.org/10.5194/egusphere-2026-2380
Preprint. Discussion started: 8 May 2026

For CO, inventory trends diverge after 2014 (CV = 15% in 2019). EDGAR and HTAPv3.2 continue to increase, while HTAPv3 shows a flattening trend. In contrast, CEDS and CAMS-GLOB-ANT exhibit decreasing emissions after 2014. Industry dominates the continued increases in HTAPv3.2 and EDGAR, whereas reductions in buildings and transport drive the declining trends in HTAPv3, CAMS-GLOB-ANT, and CEDS. TCR-3 CO estimates for 2024 exceed all bottom-up inventories and align with the extrapolated upper range represented by HTAPv3.2.

The Philippines

NO_x emissions show a consistent increasing trend after 2009, primarily driven by the transport sector, with additional contributions from the power sector. The growth rates before 2020 in CEDS and HTAP (2.8–3.8 Gg month^{-1} yr^{-1}) are approximately 2–3 times higher than those in EDGAR and CAMS-GLOB-ANT (1.4–1.7 Gg month^{-1} yr^{-1}). EDGAR and CAMS-GLOB-ANT generally report lower emissions than CEDS (highest), HTAP, and AQNEA. These differences are largely associated with the transport sector. Inter-inventory spread in 2019 is moderate (CV = 25%). TCR-3 NO_x estimates for 2024 exceed all bottom-up inventories by 30–52% (Fig. 9).

CO emissions also increase after 2009, with relatively small inter-inventory spread in 2019 (CV = 14%). AQNEA provides the lowest CO estimates for that year. The two TCR-3 products show substantial divergence: TCR-3 (MOPITT) is 30–52% lower than bottom-up inventories, whereas TCR-3 (TROPOMI) falls within the range of bottom-up estimates.

Taiwan

Taiwan shows the largest inter-inventory spread for both NO_x and CO (CV = 49% and 68%, respectively), driven primarily by CAMS-GLOB-ANT, which yields elevated estimates for both species owing to large contributions from the transport sector (CO and NO_x) and the industry sector (CO). CEDS shows the steepest NO_x decline over the period (−1.6 Gg month^{-1} yr^{-1}), followed by EDGAR (−1.1) and HTAP (−0.7). HTAP begins ~40% lower in 2000 and converges with CEDS by 2018–2019, as does AQNEA by 2019. TCR-3 in 2024 falls within the broad bottom-up spread, broadly consistent with the EDGAR trajectory.

For CO, the large inter-inventory spread and divergence in long-term trends are dominated by CAMS-GLOB-ANT, with transport sector differences as the principal driver. AQNEA lies near the center of the 2019 spread. TCR-3 (MOPITT) aligns closely with AQNEA, while TCR-3 (TROPOMI) sits at the lower end near CEDS.

South Korea

All inventories show a NO_x decline since 2015, though the rates diverge substantially (−1.3 to −5.5 Gg month^{-1} yr^{-1}). CEDS and HTAP exhibit broadly similar trends, as do CAMS-GLOB-ANT and EDGAR, although the two latter inventories diverge

https://doi.org/10.5194/egusphere-2026-2380
Preprint. Discussion started: 8 May 2026

in their absolute levels throughout the record, with EDGAR consistently the highest. The dominant declining sector also differs. Industry drives the reduction in EDGAR, whereas power dominates in CAMS-GLOB-ANT. The inter-inventory spread in 2019 is moderate (CV = 30%), with AQNEA at the lower end of the range. By 2023, CAMS-GLOB-ANT converges toward the lower-bound estimates following a steep decline attributable to reductions in transport and industry. TCR-3 in 2024 falls near the middle of the spread. Transport is the dominant NO_x source across all inventories.

For CO, the inter-inventory spread is substantially larger (CV= 61%), driven by EDGAR and CAMS-GLOB-ANT reporting values 2-4 times higher than other inventories, primarily due to large industrial emission contributions absent from regional inventories and CEDS. The two inventories also show divergent temporal behaviour: EDGAR and CAMS-GLOB-ANT exhibit increasing CO emissions between 2010 and 2015, attributable to industry and buildings sectors, whereas the remaining inventories show a continuous decline since 2000, dominated by reductions in transport. AQNEA falls between the lower-bound estimates (HTAP, CEDS) and the higher-bound estimates (EDGAR, CAMS-GLOB-ANT). TCR-3 lies at the lower end of the spread, near CEDS and HTAP.

Thailand

All inventories indicate increasing NO_x emissions in Thailand since 2000, with trend rates ranging from 0.9 to 2.1 Gg month^{-1} yr^{-1}. The inter-inventory spread remains relatively modest in 2019 (CV = 16%), with AQNEA reporting the lowest emissions, near CAMS-GLOB-ANT. TCR-3 aligns more closely with the higher-end, upward-trending HTAP and CEDS estimates.

For CO, all inventories transitioned from increasing trends in the early 2000s to decreasing trends after the mid-2010s (2012–2015), with the exception of CAMS-GLOB-ANT, which shows near-zero trend after 2016. This divergence drives a substantially wider inter-inventory spread by 2019 (CV = 48%). AQNEA reports the lowest CO in 2019. TCR-3 (MOPITT) falls near the middle of the spread, while TCR-3 (TROPOMI) lies at the lower end, close to the CEDS trajectory.

The diversity among bottom-up inventories underscores the need for continued improvement of individual products, while our top-down estimates can provide quantitative guidance on the magnitude of revisions required, albeit with their own uncertainties. Bottom-up inventories diverge because they differ in activity data, emission factors, and the spatial-temporal allocation of emissions (Solazzo et al., 2021). Activity statistics such as fuel consumption are relatively well documented for major economies but often rely on extrapolation or expert judgment in developing regions (Deng et al., 2022). Emission factors depend on technology, combustion conditions, and abatement equipment, and are inconsistently constrained by limited field measurements (Liu et al., 2015). Allocation approaches range from population-based proxies in global inventories to facility-level point sources in regional ones (Crippa et al., 2024; Gurney et al., 2019). Methodological definitions add further discrepancies: the use of Net versus Gross Calorific Values introduces 5 to 10% differences in fuel-related emissions (IPCC, 2008; Janssens-Maenhout et al., 2019), and global inventories applying Tier 1 defaults (e.g., EDGAR) systematically diverge

https://doi.org/10.5194/egusphere-2026-2380
Preprint. Discussion started: 8 May 2026

from national reports using Tier 2 or Tier 3 country-specific methods (e.g., HTAP, AQNEA) (Oda et al., 2018). The detailed comparison presented here, involving multiple bottom-up inventories and top-down constraints, helps identify priority areas for improvement and provides useful guidance for future inventory development.

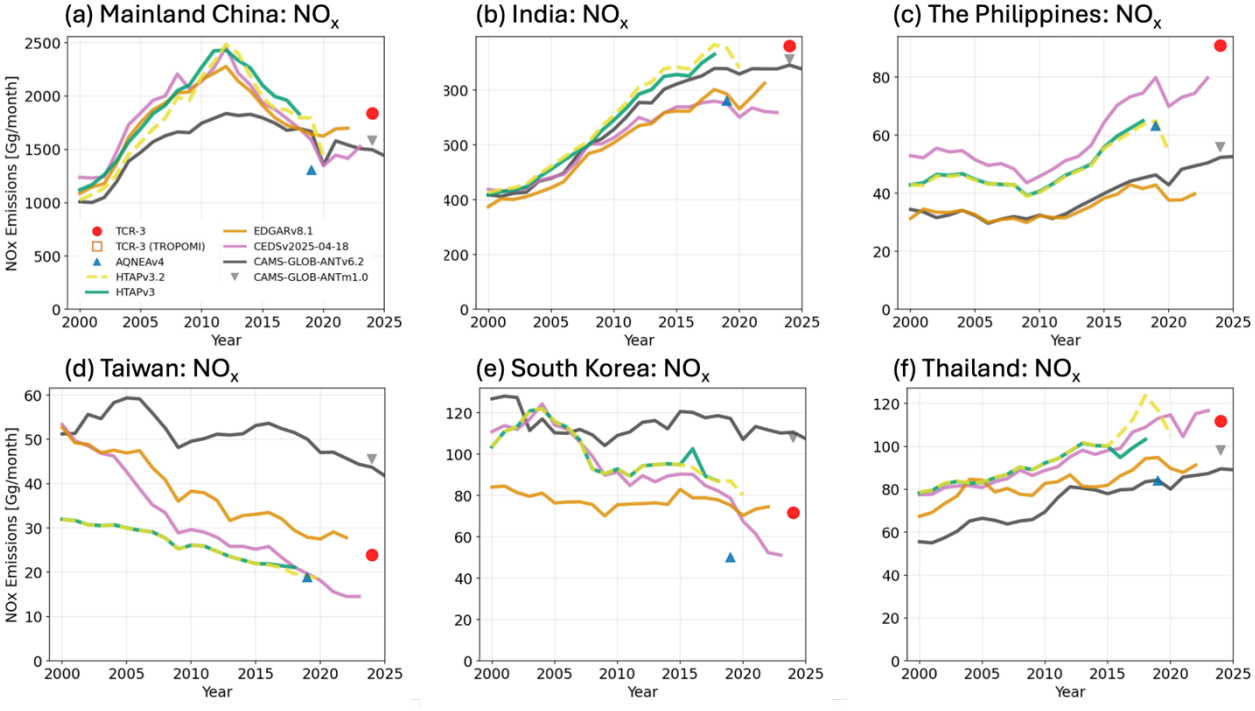

Figure 7. Time series of average February–March anthropogenic NO_x emissions across six Asian regions. The panels display monthly emissions [Gg/month] for (a) mainland China, (b) India, (c) the Philippines, (d) Taiwan, (e) South Korea, and (f) Thailand. Each region compares multiple emission inventories: TCR-3 (red circle), AQNEAv4 (blue triangle), HTAPv3.2 (yellow dashed line), HTAPv3 (green solid line), EDGARv8.1 (orange solid line), CEDSv2025-04-18 (purple solid line), CAMS-GLOB-ANTv6.2 (dark grey solid line), and CAMS-GLOB-ANTm1.0 (grey downward triangle).

https://doi.org/10.5194/egusphere-2026-2380
Preprint. Discussion started: 8 May 2026

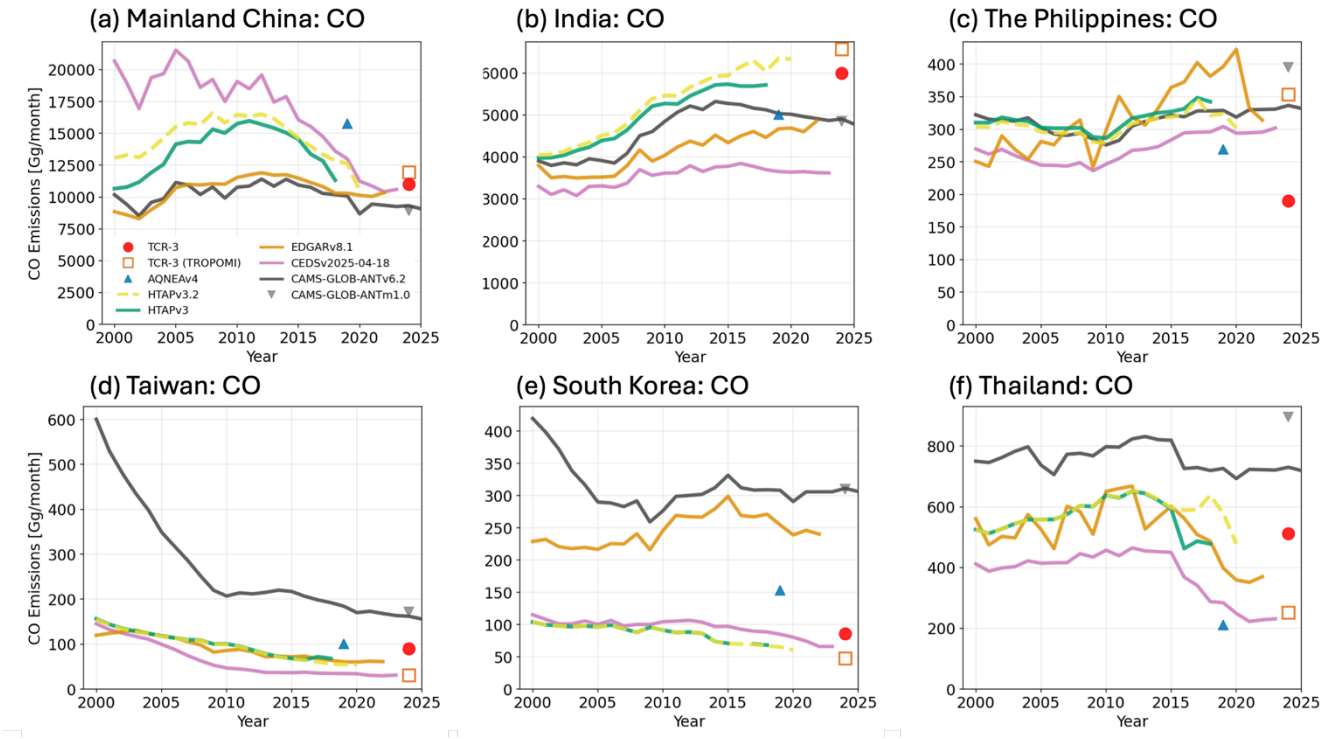

Figure 8. Same as Fig. 7 but for anthropogenic CO emissions. Each region compares multiple emission inventories, including TCR-3 (MOPITT) (red circle) and TCR-3 (TROPOMI) (open orange square).

https://doi.org/10.5194/egusphere-2026-2380
Preprint. Discussion started: 8 May 2026

551
552

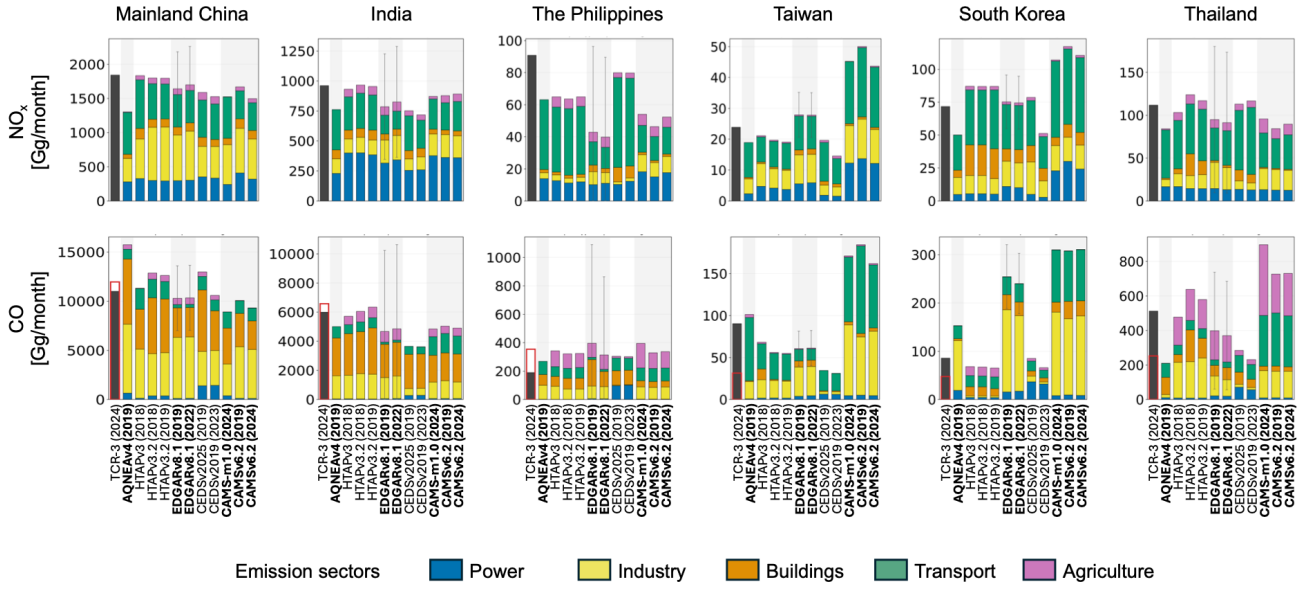

553

554 **Figure 9.** Regional total anthropogenic emissions of NO_x (top row) and CO (bottom row) during February–March 2024,
555 expressed in Gg/month for mainland China, India, the Philippines, Taiwan, South Korea, and Thailand. Bars are grouped by
556 inventory: TCR-3 (2024), AQNEAv4 (2019), HTAPv3 (2018), HTAPv3.2 (2018 and 2019), EDGARv8.1 (2019 and 2022),
557 CEDSv2025-04-18 (2019 and 2023), CAMS-GLOB-ANTm1.0 (2024), and CAMS-GLOB-ANTv6.2 (2019 and 2024).
558 CAMS-GLOB-ANTm1.0 and v6.2 are the only inventories covering 2024, the target year of TCR-3 and ASIA-AQ. For CO
559 panels, open red squares on the TCR-3 (2024) bars indicate the TCR-3 (TROPOMI) values. Stacked color indicates the sectoral
560 contribution: Power (blue), Industry (yellow), Buildings (orange), Transport (green), and Agriculture (purple). TCR-3 (2024)
561 does not provide sectoral information and is shown in dark grey. The TCR-3 prior excludes agricultural emissions to avoid
562 double-counting with biomass burning emissions. Error bars represent 1-sigma EDGAR uncertainties from Table S3 of Crippa
563 et al. (2019), ranging from 26–125% for NO_x and 26–175% for CO depending on the region. Alternating white and light-grey
564 background shading visually separate inventory groups.

https://doi.org/10.5194/egusphere-2026-2380
Preprint. Discussion started: 8 May 2026

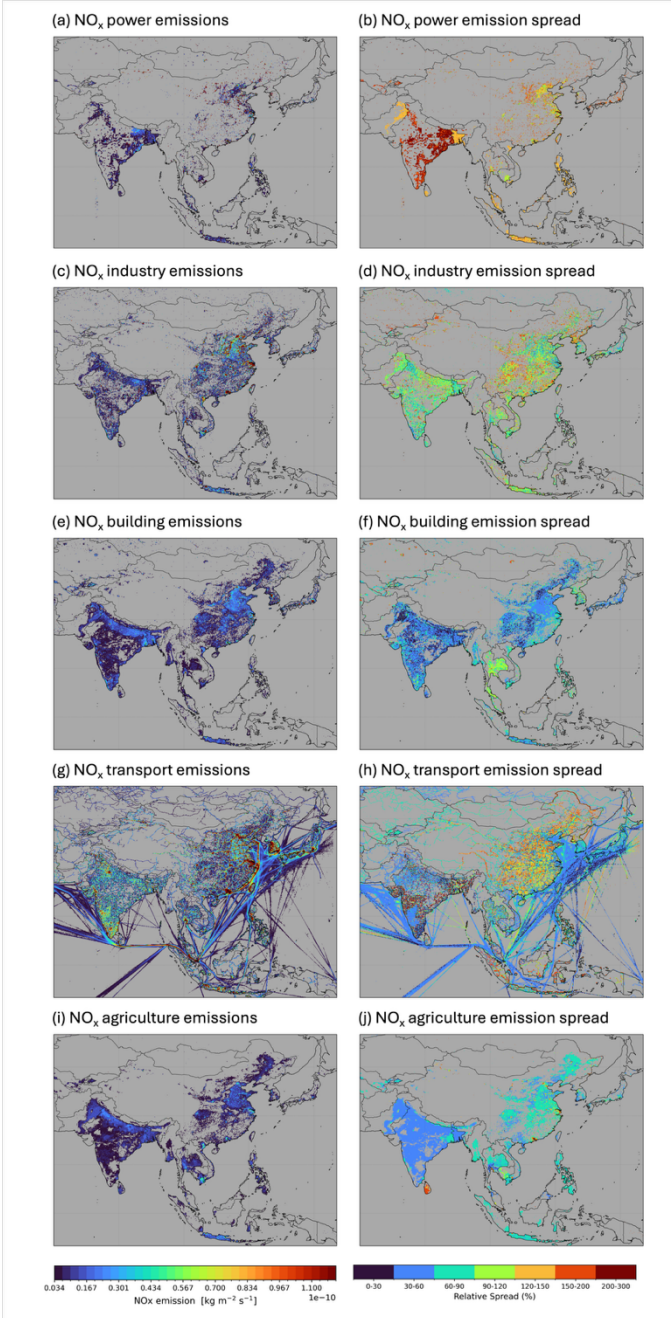

Figure 10. Mean sectoral NOx emissions (a,c,e,g,i) and Inter-inventory coefficient of variation (CV, %) (b,d,f,h,j) for Feb-Mar 2019 at 0.1° × 0.1° resolution by sector: Power (a, b), Industry (c, d), Buildings (e, f), Transportation (g, h), and Agriculture (i, j). Mean and CV are calculated from five inventories with base year 2019: AQNEAv4, HTAPv3.2, EDGARv8.1, CEDSv2025-04-18, and CAMS-GLOB-ANTv6.2. CV is shown only for grid cells where mean emissions exceed a minimum threshold (0.034e-10 kg m^{-2} s^{-1}).

https://doi.org/10.5194/egusphere-2026-2380
Preprint. Discussion started: 8 May 2026

4.2 Biomass burning emissions

We compare our top-down biomass burning emissions with GFASv1.2 (Kaiser et al., 2012), GFED4 (Giglio et al., 2013), the Fire INventory from NCAR version 2.7 (FINNv2.7) (Wiedinmyer et al., 2023; Maneenoi et al., submitted), and the Quick Fire Emissions Dataset version 2.6 R1 (QFEDv2.6r1) (Koster et al., 2015). GFASv1.2 assimilates Moderate Resolution Imaging Spectroradiometer (MODIS) fire radiative power (FRP) observations to estimate dry matter combustion rates and applies biome-specific emission factors to derive trace gas and aerosol fluxes. GFED4 combines MODIS burned area maps with active fire data from the Tropical Rainfall Measuring Mission (TRMM) Visible and Infrared Scanner (VIRS) and the Along-Track Scanning Radiometer (ATSR) family of sensors. FINNv2.7 combines Visible Infrared Imaging Radiometer Suite (VIIRS) and Himawari-9 Advanced Himawari Imager (AHI) active fire detections with land cover data, emission factors from the NEIVAv1.0 database (Binte Shahid et al., 2024), and fuel loadings to produce daily emissions. Compared to FINNv2.5, FINNv2.7 applies a corrected Himawari pixel size consistent with VIIRS and uses a proximity filter to remove duplicated and nearby detections, leading to reduced emissions overall (Maneenoi et al., submitted; Fig. S5). QFEDv2.6r1 derives emissions from FRP observations using biome-specific coefficients optimized to reproduce observed aerosol optical depth patterns.

The largest emitters are Laos, Myanmar, and India, followed by mainland China and Cambodia (Fig. 11). Substantial differences are evident among the three inventories. FINNv2.7 yields CO emissions larger by a factor of 2–5 across Southeast Asia relative to GFASv1.2, GFED4, and QFEDv2.6r1. Also, FINNv2.7 derives emissions from satellite fire detections including VIIRS and hourly Himawari-9 sensors, providing greater sensitivity to small, fragmented, and local evening crop burning that are common in Southeast Asia (Liu et al., 2020; Marvin et al., 2024; Maneenoi et al., submitted). In contrast, FRP based inventories that rely on biome dependent or globally uniform conversion factors (GFAS and QFED) tend to produce lower emissions, particularly where agricultural burning dominates, cloud and haze obscure active fires, or combustion occurs at low intensity.

For the top-down CO emission estimates, we use two different configurations: one based on MOPITT CO assimilation with daily GFASv1.2 emissions as the prior, and the other based on TROPOMI CO assimilation with monthly GFED4 emissions as the prior. Because both the assimilated observations and the prior emissions influence the inferred emissions, dedicated sensitivity experiments in which these factors are varied separately would be required to isolate their individual roles. In the present study, these two configurations are used to characterize the range of uncertainty in the estimated emissions arising from different assimilation settings (Fig. S6). The inversion increases the biomass burning fraction of total CO from 14.4% (GFASv1.2 prior) to 24.0% for TCR-3 (MOPITT) and from 17.3% (GFED4 prior) to 36.9% for TCR-3 (TROPOMI). TCR-3 (TROPOMI) yields biomass burning CO emissions roughly twice those of TCR-3 (MOPITT) over Asia (31 vs 15 Tg), despite a 15% lower prior, indicating that TROPOMI detects substantially larger fire-related CO enhancements (Fig. S7). Across the major biomass burning regions, TCR-3 (MOPITT) generally exceeds GFASv1.2 by a factor of 1.5–3 (excepts over Indonesia). TCR-3 (TROPOMI) substantially exceeds GFED4 across all major regions by factors of 2–8. FINNv2.7 exceeds TCR-3 (MOPITT) by a factor of 1.3–5, but agrees closely with TCR-3 (TROPOMI) across the major burning regions.

https://doi.org/10.5194/egusphere-2026-2380
Preprint. Discussion started: 8 May 2026

Thailand experienced the most severe AQ conditions during the ASIA-AQ period, driven by intense biomass burning in the north. Figure 12 shows daily CO fire emissions for two subregions: northern Thailand and surrounding regions (NTHA, above 16°N) and southern Thailand and surrounding regions (STHA, below 16°N). In the NTHA region, emissions peak in early to mid-March, coinciding with the ASIA-AQ observation period (March 13–27, shaded). The STHA region shows much lower fire emissions across all inventories throughout the period.

TCR-3 (MOPITT) and TCR-3 (TROPOMI) increase biomass burning CO emissions over the NTHA and STHA domains relative to their respective prior inventories, from 3.6 (GFASv1.2) to 8.3 Tg and 5.6 (GFED4) to 14.5 Tg, respectively, roughly a factor of 2–3. FINNv2.7 emissions are substantially higher than both TCR-3 products at 17.9 Tg. The biomass burning fraction of total CO emissions increases substantially with assimilation in both configurations (Fig. S7), with TCR-3 (TROPOMI) showing particularly large enhancements concentrated in North and West Thailand. TCR-3 (MOPITT) captures the day-to-day evolution of fire activity, increasing emissions relative to GFASv1.2. TCR-3 (TROPOMI), by contrast, uses monthly GFED4 as its prior and therefore does not resolve day-to-day fire variability. The assimilated TROPOMI CO column nevertheless produces general enhancements in emissions during early-to-mid March, particularly over NTHA. The contrasting emission estimates between the two TCR-3 configurations are reflected in their surface CO performance over Thailand, where TCR-3 (MOPITT) reduces the surface negative bias while TCR-3 (TROPOMI) overestimates surface concentrations despite better capturing elevated CO aloft, as discussed in Section 3.1.

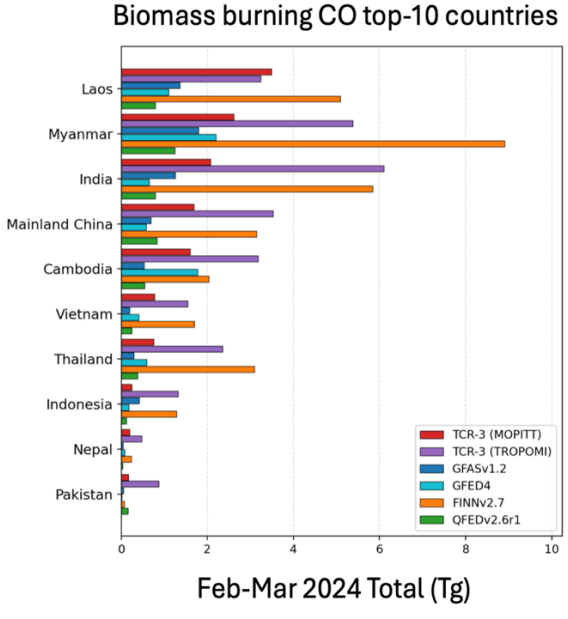

Figure 11. Total CO emissions (Tg) from the ten highest-emitting regions within our study domain (Fig. 6) where the order follows TCR-3 (MOPITT). Bars represent six different emission inventories: TCR-3 (MOPITT) (red), TCR-3 (TROPOMI) (purple), GFASv1.2 (blue), GFED4 (cyan), FINNv2.7 (orange), and QFEDv2.6r1 (green).

https://doi.org/10.5194/egusphere-2026-2380
Preprint. Discussion started: 8 May 2026

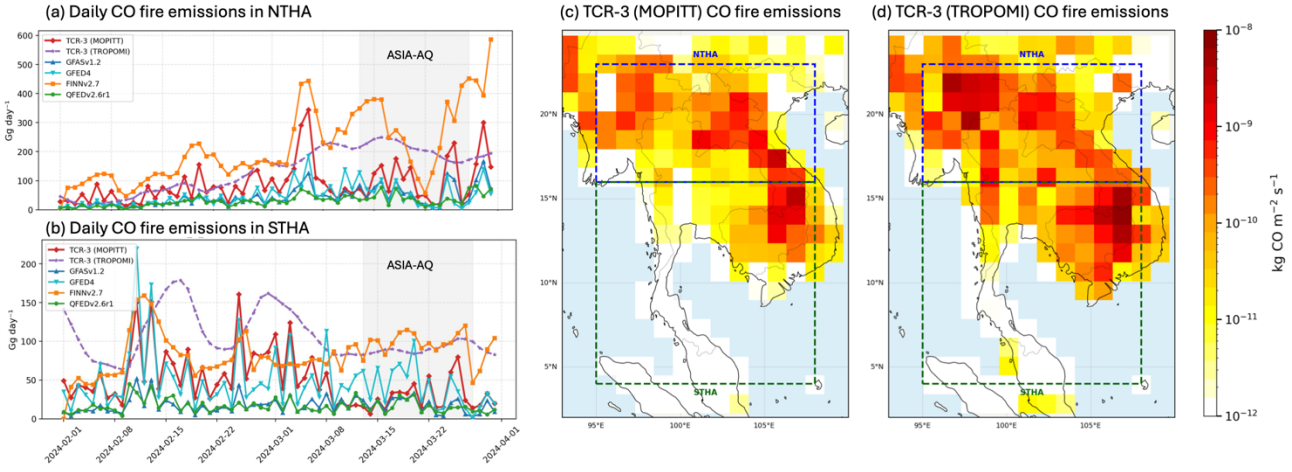

Figure 12. Daily CO fire emissions (Gg/day) in (a) northern Thailand and surrounding regions (NTHA; north of 16°N), and (b) southern Thailand and surrounding regions (STHA; south of 16°N) during February–March 2024. The shaded grey period (March 13–27) indicates the ASIA-AQ observation period in Thailand. Lines represent four biomass-burning emission inventories: TCR-3 (MOPITT) (red), TCR-3 (TROPOMI) (purple), GFASv1.2 (blue), GFED4 (cyan), FINNv2.7 (orange), and QFEDv2.6r1 (green). Spatial distribution of (c) TCR-3 (MOPITT) and (d) TCR-3 (TROPOMI) CO fire emissions (kg CO m^{-2} s^{-1}) averaged over February–March 2024, with the NTHA (blue box) and STHA (green box) subregions marked.

5. Local and transboundary transport

To understand the sources contributing to O_3 pollution across the ASIA-AQ regions and to quantify the influence of transboundary transport, we conduct a series of emission perturbation experiments for CO, NO_x, and isoprene. These experiments employ two scenarios: a 20% emission reduction to evaluate the surface O_3 response to near-future mitigation strategies, and a 100% emission reduction (zero-out) to maximize the signal of specific sources. Perturbations are applied individually to ten source regions (Fig. S8): South Korea, Philippines, Taiwan, Thailand, mainland China, India, Myanmar, Laos, Vietnam, and Rest of Southeast Asia. While assessing the impacts of specific policy measures would require more targeted and sector-resolved sensitivity experiments, these perturbations are designed to provide a first-order, domain-wide quantification of the relative importance of regional source contributions.

5.1 Surface O_3

Figure 13 shows the daily surface O_3 response in five receptor cities (Seoul, Chiang Mai, Taipei, Manila, and Bangkok) to 20% emission reductions applied separately to each source region, representing a near-future mitigation scenario. The 100% emission reduction (zero-out) results are shown in Fig. S9 for reference. A comparison between the two experiments reveals substantial nonlinearity in the O_3 response, particularly over Seoul and Taipei, where the 100% response is not proportional to

https://doi.org/10.5194/egusphere-2026-2380
Preprint. Discussion started: 8 May 2026

the 20% response. For example, over Seoul on February 11, removing 100% of mainland China emissions produces an O_3 response of ~−30 ppbv, whereas a 20% reduction yields only ~−2 ppbv, far less than one-fifth of the zero-out response, reflecting NO_x-saturated photochemical conditions and the nonlinear sensitivity of O_3 to precursor emissions. In general, foreign emission contributions appear larger in the 100% sensitivity simulation, showing that the 20% reduction results presented here provide a conservative and policy-relevant estimate of transboundary influences under realistic mitigation scenarios.

Over Manila, the relative importance of transported pollution varies strongly with meteorological regimes. The DC-8 flight dates over the Philippines captured two distinct regimes. The first two flights (February 6–7) occurred under a weak Northeast (NE) Monsoon, when local emissions dominate O_3 formation, The latter two flights (February 11, and 13) coincided with an enhanced NE Monsoon (northeasterly) that enabled substantial long-range transport, accounting for up to 62% of the total O_3 response, with the largest contribution from mainland China (18%). This contrast underscores the controlling role of synoptic-scale circulation in modulating O_3 over Manila.

Taipei and Seoul show O_3 increases and decreases in response to emission reductions. Over Taipei, the DC-8 flight dates corresponded to contrasting meteorological conditions: pre-frontal conditions on February 15, when local emissions dominated O_3 formation, versus post-frontal northwesterly flow on March 13 and 27, when transport from mainland China dominated. Over Seoul, O_3 increases in response to local emission reductions throughout the period, reflecting NO_x-saturated conditions. Seoul's response to Chinese emissions varies according to wind directions, typically showing decreases when transport originates from the North China Plain but increases when influenced by less polluted source regions.

Bangkok and Chiang Mai are strongly influenced by local emissions, but exhibit distinct transboundary signals. Over Bangkok, transport from Vietnam becomes important during southerly maritime flow. In contrast, Chiang Mai is primarily influenced by inflow from Myanmar, Laos, and India. Chiang Mai experiences the most severe biomass burning impacts during periods flagged for enhanced combustion and smoke (Figure 2). During these fire episodes, Myanmar becomes the dominant external source, with contributions exceeding those from local Thailand emissions. During March 21–23, a mid-latitude synoptic system over northern Thailand brought more diverse foreign influences, including mainland China.

https://doi.org/10.5194/egusphere-2026-2380
Preprint. Discussion started: 8 May 2026

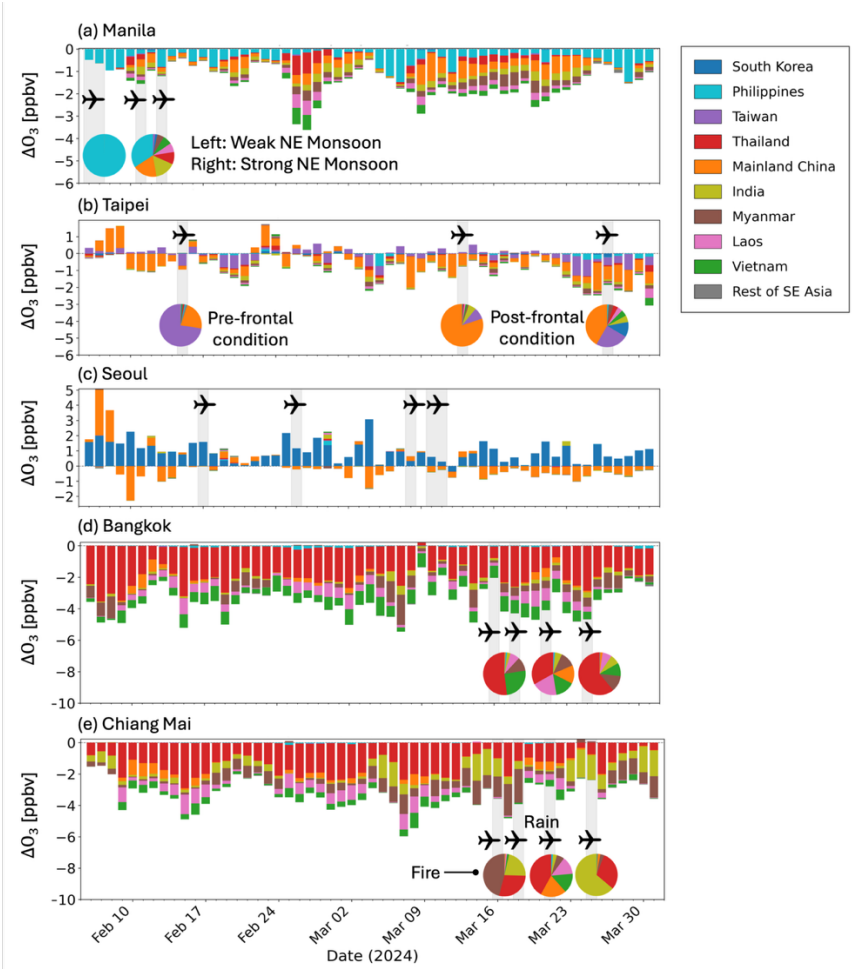

Figure 13. Regional contributions to daily surface O_3 concentrations in five cities based on 20% combined emission reduction sensitivity experiments. Panels show results for (a) Manila, (b) Taipei, (c) Seoul, (d) Bangkok, and (e) Chiang Mai. Stacked bars represent the daily change in surface O_3 (ΔO_3, ppbv) when CO, NO_x, and isoprene emissions from each source region are simultaneously reduced by 20%. Colors indicate different source regions: South Korea (blue), Philippines (teal), Taiwan (purple), Thailand (red), mainland China (orange), India (olive), Myanmar (brown), Laos (pink), Vietnam (green), and Rest of Southeast Asia (grey). Negative values indicate O_3 decreases resulting from emission reductions, while positive values indicate nonlinear O_3 responses to precursor emission changes. Grey shading with airplane icons marks DC-8 flight dates during ASIA-AQ. Pie charts show the relative contributions from each region during selected flight periods: weak versus strong northeast monsoon conditions in Manila (a), pre-frontal versus post-frontal conditions in Taipei (b), and biomass burning versus cleaner periods in Bangkok and Chiang Mai (d-e). No pie chart is shown for Seoul (c) due to the nonlinear response where local emission reductions (South Korea) lead to O_3 increases rather than decreases.

https://doi.org/10.5194/egusphere-2026-2380
Preprint. Discussion started: 8 May 2026

5.2 Influences from India

Although India lies outside the ASIA-AQ domain, rapid economic growth and associated emission increases raise concerns for both domestic air quality and downwind regions (Ding et al., 2022; Guizzardi et al., 2025; Kurokawa and Ohara, 2020; Soulie et al., 2024). Despite national mitigation efforts such as the National Clean Air Programme (NCAP) (Guttikunda et al., 2023), substantial health burdens and high levels of O_3 and its precursors remain (Gopikrishnan et al., 2025; Gopikrishnan and Kuttippurath, 2024). Beyond domestic impacts, Indian emissions can influence regional atmospheric composition through frequent deep convection, which lofts pollutants into the free troposphere and facilitates long-range transport toward Southeast and East Asia (Lawrence and Lelieveld, 2010; Lelieveld et al., 2001).

While Indian emissions play a relatively minor role in surface O_3 across most of the ASIA-AQ domain, their influence becomes substantial aloft. Figure 14 illustrates the Indian emission contribution to mid-tropospheric O_3 at 500 hPa, showing the O_3 response to 100% emission reductions averaged over March 21–25, 2024, when the Indian influence was particularly strong. The response extends from the Indian subcontinent across the Bay of Bengal into Southeast Asia and southern China, reaching as far as Seoul. The spatial pattern suggests that polluted air is being lofted by deep convection over Northeast India and the Himalayan foothills and subsequently transported eastward in the mid-troposphere.

Downwind O_3 enhancements may reflect both O_3 produced over India and the export of precursors, such as peroxyacetyl nitrate (PAN), which releases NO_x and promotes O_3 production during transport. Observations of PAN (Payne et al., 2022a) from the Cross-Track Infrared Sounder (CrIS) (Shephard and Cady-Pereira, 2015) reveal elevated concentrations along the simulated transport pathway (Fig. S10). These elevated PAN levels provide independent evidence for the efficient long-range export of both O_3 and its precursors. The thermal stability and persistence of PAN under cold upper-tropospheric conditions facilitate its transport over long distances, potentially extending to trans-Pacific scales where subsequent subsidence and warming release NO_x to produce O_3 in downwind receptor regions.

The time series for Taipei, Chiang Mai, and Seoul suggest that the Indian emission contribution to 500 hPa O_3 peaks during March 21–25, 2024. At peak influence, Indian emissions account for 78%, 72%, and 24% of the total O_3 response at 500 hPa in Taipei (March 21), Chiang Mai (March 25), and Seoul (March 24-25), respectively. These large contributions at considerable distances from the source underscore the efficiency of convective lofting and mid-tropospheric transport in delivering Indian emissions to remote receptors. Although the surface O_3 impact across the ASIA-AQ domain is generally limited, Indian emissions can make a substantial contribution to mid-tropospheric O_3 during active convective period, with potential surface impacts through vertical mixing during convective events or frontal passages.

https://doi.org/10.5194/egusphere-2026-2380
Preprint. Discussion started: 8 May 2026

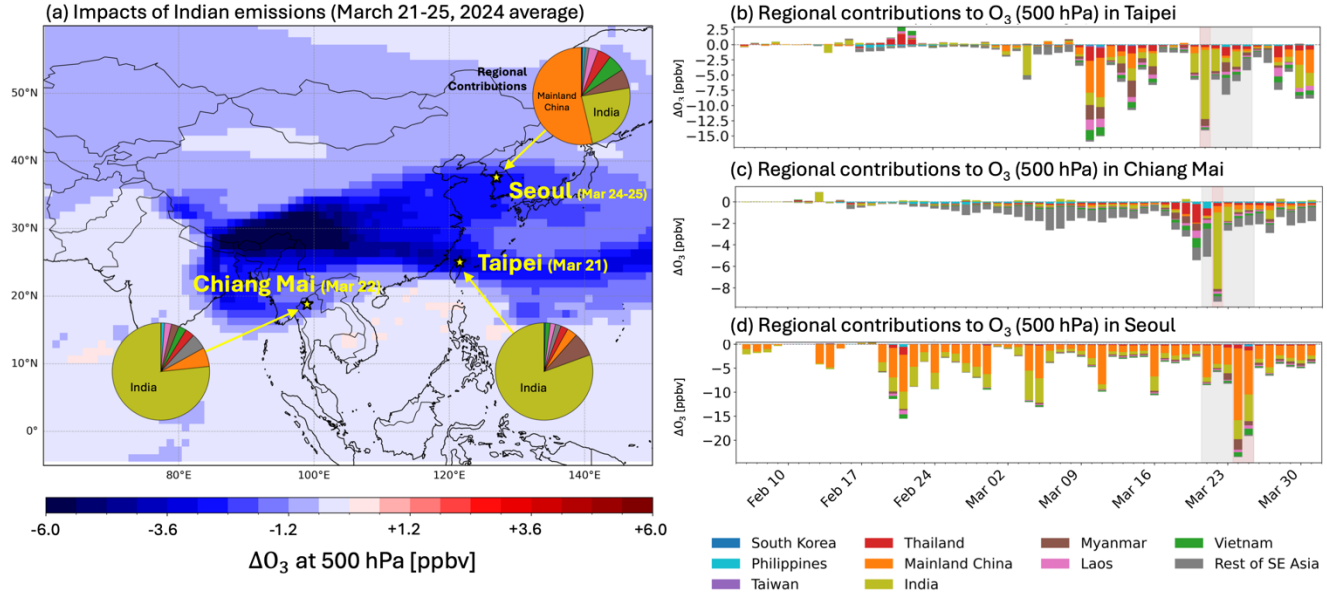

Figure 14. Impact of Indian emissions on mid-tropospheric O_3 (500 hPa) over East and Southeast Asia. (a) Spatial distribution of ΔO_3 at 500 hPa averaged over March 21–25, 2024, resulting from 100% reduction of Indian CO, NO_x, and isoprene emissions. Yellow stars mark three cities where Indian impacts are examined: Seoul, Taipei, and Chiang Mai. Pie charts show the relative regional contributions to 500 hPa O_3 during peak Indian influence periods (dates in parentheses). (b-d) Time series of daily changes in 500 hPa O_3 (ΔO_3, ppbv) from 100% combined emission reductions in each source region for (b) Taipei, (c) Chiang Mai, and (d) Seoul. Stacked bars show contributions from different regions using the same color scheme as Fig. 13. Grey shading indicates March 21–25, when Indian impacts were widespread across the domain. Red shading highlights peak Indian influence periods at each city, corresponding to the dates shown in panel (a).

6. Conclusions

To advance understanding of air pollutants drivers across East and Southeast Asia, we utilize the TCR-3 chemical reanalysis, produced using the MOMO-Chem data assimilation framework, which integrates multiple satellite observations during the ASIA-AQ campaign (February–March 2024). The comprehensive ASIA-AQ measurements provide a unique opportunity to evaluate chemical reanalysis performance, assess bottom-up emission inventories, and quantify the value of satellite observing systems, aimed at supporting air quality management in Asia.

Evaluations against DC-8 aircraft measurements demonstrates that the data assimilation improves agreement for O_3, NO_x, CO, and CH_2O across the campaign domain. The largest gains are for CO and CH_2O. CO correlations increase from 0.63–0.64 to 0.77, while NMB is reduced from −32–33% to −15–16% across the domain. The most substantial regional improvement occurs

https://doi.org/10.5194/egusphere-2026-2380
Preprint. Discussion started: 8 May 2026

over Thailand, where the correlation increases from 0.07 to 0.50 below 1 km and surface NMB improves from −28% to −8%, reflecting improved representation of episodic biomass burning enhancements. Modest but consistent improvements are also evident over the Philippines and Taiwan. For CH_2O, the positive model biases are reduced from 55–70% to 17–29% across the domain, with the largest corrections over the Philippines (NMB from +74% to +22% below 1 km), Taiwan (+109% to +48%), and Thailand (+87% to +43%), consistent with the reduced isoprene emission by data assimilation.

The optimized emissions emission estimates reveal substantial discrepancies with existing bottom-up inventories. TCR-3 NO_x exceeds both global (EDGAR, CEDS, and CAMS-GLOB-ANT) and regional (HTAP, AQNEA) inventories by 30–52% over the Philippines and lies at the upper end of bottom-up estimates over mainland China, suggesting potential underestimation of transport emissions in bottom-up inventories. For anthropogenic CO emissions, EDGAR and CAMS-GLOB-ANT estimates over South Korea and Taiwan are 2–4 times higher than both TCR-3 and regional inventories, where other inventories lack large industrial sector contributions. In India, TCR-3 anthropogenic CO exceeds all bottom-up inventories, aligning with the extrapolated upper range of HTAPv3.2, suggesting continued industry-driven emission growth beyond recent inventory updates.

Biomass burning emissions show even larger discrepancies. Northern Thailand experienced the most severe air quality conditions during the ASIA-AQ period, with biomass burning CO emissions reaching 5.3 and 8.1 Tg for TCR-3 (MOPITT) and TCR-3 (TROPOMI), respectively, out of regional totals of 15.0 and 30.5 Tg across Northeast and Southeast Asia. Across the broader region, bottom-up inventories range from 5.8 Tg (QFEDv2.6r1) to 34.0 Tg (FINNv2.7), highlighting persistent uncertainties in fire emission estimates. The 53% domain-wide reduction in isoprene emissions inferred by TCR-3 support earlier findings that MEGAN overestimates biogenic fluxes in tropical Southeast Asia (Choi et al., 2025; Sindelarova et al., 2014), with important implications for O_3 formation. Overall, the substantial emission adjustments indicated by TCR-3 underscore the limitations of bottom-up inventories in capturing rapidly evolving emission patterns across Asia.

In addition to local emissions, transboundary transport plays a highly variable and often dominant role in shaping air quality across the ASIA-AQ domain. Over Manila, long-range transport accounts for up to 62% of the surface O_3 response during enhanced northeast monsoon conditions (Feb 11), with mainland China as the largest single foreign contributor (~18%). Over Bangkok, Vietnamese emissions become important during southerly maritime flow, while Chiang Mai is primarily influenced by inflow from Myanmar, Laos, and India, with Myanmar emerging as the dominant external source during intense fire episodes in March, exceeding even local Thailand contributions. Notably, Indian emissions exert a substantial influence in the free troposphere, contributing 78%, 72%, and 24% of the O_3 response over Taipei, Chiang Mai, and Seoul during March 21–25, likely reflecting deep convective lofting of precursors over the Indian subcontinent and subsequent eastward transport. These results highlight the importance of three-dimensional transport pathways and cross-border precursor contributions, emphasizing the need for coordinated international air quality management strategies.

https://doi.org/10.5194/egusphere-2026-2380
Preprint. Discussion started: 8 May 2026

This study demonstrates the value of integrating multi-platform satellite observations with aircraft campaigns like ASIA-AQ to address three key scientific challenges: sparse ground-based monitoring, uncertain bottom-up inventories, and complex transboundary transport. Emerging satellite measurements provide significant opportunities for future improvements. Geostationary instruments such as GEMS enable hourly observations of NO_2 and CH_2O over Asia (Kwon et al., 2019; Lee et al., 2024; Seo et al., 2024), while Himawari-9 provides high-resolution aerosol data; together, these could further constrain the diurnal variability in emissions and photochemistry that our analysis has shown to be important (Yang et al., 2024). CrIS retrievals of O_3 (Boynard et al., 2025), CO (Fu et al., 2016; Worden et al., 2022), PAN (Payne et al., 2022b), ammonia (NH_3) (Cady-Pereira et al., 2024), and isoprene (Fu et al., 2019; Wells et al., 2020, 2022), and other NMVOCs (Brewer et al., 2024; Wells et al., 2025) can further improve emission estimates and chemical processes. In particular, NH_3, a key precursor of inorganic aerosols whose emissions remain highly uncertain (Cao et al., 2020), is not addressed in this study. Fully exploiting these observations will require continued advances in data assimilation methods and model process representation.

Data availability

Tropospheric Chemistry Reanalysis are available at https://doi.org/10.25966/9qgv-fe81 (Miyazaki et al.. 2019) and on the NASSA GES DISC website (https://disc.gsfc.nasa.gov/information/data-release?title=Release%20of%20TROPESS%20Chemical%20Reanalysis%20Products). ASIA-AQ DC-8 airborne observations are open access and available in the ASIA-AQ Data Archive (https://doi.org/10.5067/SUBORBITAL/ASIA-AQ/DATA001, ASIA-AQ Science Team, 2024).

Author contributions

Conceptualization: JC and KM. Methodology & Software: JC, KM, and TS. Investigation: JC, KM, TS, RB, AR, LKn, GSD, JAM, JPD, YC, AF, CC, ECA, JMSC, RAH, GMW, ED, AS, and DRB. Formal Analysis & Visualization: JC. Resources & Data Curation: JC, KM, TS, HE, PR, LKE, NM, MC, RMH, SJS, JHW, and LKu. Writing – Original Draft: JC. Writing – Review & Editing: All coauthors.

https://doi.org/10.5194/egusphere-2026-2380
Preprint. Discussion started: 8 May 2026

Acknowledgements

This work was supported by an appointment to the NASA Postdoctoral Program at the NASA Jet Propulsion Laboratory, administered by ORAU under contract with NASA. Part of this research was carried out at the Jet Propulsion Laboratory, California Institute of Technology, under contract with the National Aeronautics and Space Administration (80NM0018D0004). We acknowledge the use of data products from NASA (Aura and EOS Terra and Aqua satellite missions). We also acknowledge the support of the NASA Atmospheric Composition: Aura Science Team Program (19-AURAST19-0044), Earth Science U.S. Participating Investigator program (22-EUSPI22-0005), ACMAP (22-ACMAP22-0013), and the NASA TROPESS project. The ROZE and ISAF teams acknowledge support from the NASA Tropospheric Composition Program. Contributions to this work were funded by NASA ASIA-AQ Award 80NSSC23K0823 (LKE and NM). This work was also supported by the NSF National Center for Atmospheric Research, which is a major facility sponsored by the U. S. National Science Foundation under Cooperative Agreement No. 1852977.

References

ASEAN Secretariat: Guidelines for the Implementation of the ASEAN Policy on Zero Burning, ASEAN Secretariat, Jakarta, 2003.

ASEAN Secretariat: ASEAN Peatland Management Strategy 2023-2030, ASEAN Secretariat, Jakarta, 2023.

Binte Shahid, S., Lacey, F. G., Wiedinmyer, C., Yokelson, R. J., and Barsanti, K. C.: NEIVAv1.0: Next-generation Emissions InVentory expansion of Akagi et al. (2011) version 1.0, Geoscientific Model Development, 17, 7679–7711, https://doi.org/10.5194/gmd-17-7679-2024, 2024.

Bocquet, M., Elbern, H., Eskes, H., Hirtl, M., Žabkar, R., Carmichael, G. R., Flemming, J., Inness, A., Pagowski, M., Pérez Camaño, J. L., Saide, P. E., San Jose, R., Sofiev, M., Vira, J., Baklanov, A., Carnevale, C., Grell, G., and Seigneur, C.: Data assimilation in atmospheric chemistry models: current status and future prospects for coupled chemistry meteorology models, Atmospheric Chemistry and Physics, 15, 5325–5358, https://doi.org/10.5194/acp-15-5325-2015, 2015.

Borsdorff, T., Aan de Brugh, J., Hu, H., Aben, I., Hasekamp, O., and Landgraf, J.: Measuring Carbon Monoxide With TROPOMI: First Results and a Comparison With ECMWF-IFS Analysis Data, Geophysical Research Letters, 45, 2826–2832, https://doi.org/10.1002/2018GL077045, 2018.

Bousserez, N., Henze, D. K., Rooney, B., Perkins, A., Wecht, K. J., Turner, A. J., Natraj, V., and Worden, J. R.: Constraints on methane emissions in North America from future geostationary remote-sensing measurements, Atmospheric Chemistry and Physics, 16, 6175–6190, https://doi.org/10.5194/acp-16-6175-2016, 2016.

Boynard, A., Wespes, C., Hadji-Lazaro, J., Sinnathamby, S., Hurtmans, D., Coheur, P.-F., Doutriaux-Boucher, M., Onderwaater, J., Steinbrecht, W., Pennington, E. A., Bowman, K., and Clerbaux, C.: Assessment of 16-year tropospheric ozone trends from the IASI Climate Data Record, Atmospheric Chemistry and Physics, 25, 11719–11755, https://doi.org/10.5194/acp-25-11719-2025, 2025.

https://doi.org/10.5194/egusphere-2026-2380
Preprint. Discussion started: 8 May 2026

838 Brewer, J. F., Millet, D. B., Wells, K. C., Payne, V. H., Kulawik, S., Vigouroux, C., Cady-Pereira, K. E., Pernak, R., and Zhou,
839 M.: Space-based observations of tropospheric ethane map emissions from fossil fuel extraction, Nat Commun, 15, 7829,
840 https://doi.org/10.1038/s41467-024-52247-z, 2024.

841 Cady-Pereira, K. E., Guo, X., Wang, R., Leytem, A. B., Calkins, C., Berry, E., Sun, K., Müller, M., Wisthaler, A., Payne, V.
842 H., Shephard, M. W., Zondlo, M. A., and Kantchev, V.: Validation of MUSES NH_3 observations from AIRS and CrIS against
843 aircraft measurements from DISCOVER-AQ and a surface network in the Magic Valley, Atmospheric Measurement
844 Techniques, 17, 15–36, https://doi.org/10.5194/amt-17-15-2024, 2024.

845 Cao, C., De Luccia, F. J., Xiong, X., Wolfe, R., and Weng, F.: Early On-Orbit Performance of the Visible Infrared Imaging
846 Radiometer Suite Onboard the Suomi National Polar-Orbiting Partnership (S-NPP) Satellite, IEEE Transactions on Geoscience
847 and Remote Sensing, 52, 1142–1156, https://doi.org/10.1109/TGRS.2013.2247768, 2014.

848 Cao, H., Henze, D. K., Shephard, M. W., Dammers, E., Cady-Pereira, K., Alvarado, M., Lonsdale, C., Luo, G., Yu, F., Zhu,
849 L., Danielson, C. G., and Edgerton, E. S.: Inverse modeling of NH3 sources using CrIS remote sensing measurements, Environ.
850 Res. Lett., 15, 104082, https://doi.org/10.1088/1748-9326/abb5cc, 2020.

851 Cazorla, M., Wolfe, G. M., Bailey, S. A., Swanson, A. K., Arkinson, H. L., and Hanisco, T. F.: A new airborne laser-induced
852 fluorescence instrument for in situ detection of formaldehyde throughout the troposphere and lower stratosphere, Atmospheric
853 Measurement Techniques, 8, 541–552, https://doi.org/10.5194/amt-8-541-2015, 2015.

854 Chan, K. L., Valks, P., Heue, K.-P., Lutz, R., Hedelt, P., Loyola, D., Pinardi, G., Van Roozendael, M., Hendrick, F., Wagner,
855 T., Kumar, V., Bais, A., Piters, A., Irie, H., Takashima, H., Kanaya, Y., Choi, Y., Park, K., Chong, J., Cede, A., Frieß, U.,
856 Richter, A., Ma, J., Benavent, N., Holla, R., Postylyakov, O., Rivera Cárdenas, C., and Wenig, M.: Global Ozone Monitoring
857 Experiment-2 (GOME-2) daily and monthly level-3 products of atmospheric trace gas columns, Earth System Science Data,
858 15, 1831–1870, https://doi.org/10.5194/essd-15-1831-2023, 2023.

859 Choi, J., Henze, D. K., Nawaz, M. O., and Malley, C. S.: Source Attribution of Health Burdens From Ambient PM2.5, O3,
860 and NO2 Exposure for Assessment of South Korean National Emission Control Scenarios by 2050, GeoHealth, 8,
861 e2024GH001042, https://doi.org/10.1029/2024GH001042, 2024.

862 Choi, J., Henze, D. K., Wells, K. C., and Millet, D. B.: Joint Inversion of Satellite-Based Isoprene and Formaldehyde
863 Observations to Constrain Emissions of Nonmethane Volatile Organic Compounds, JGR Atmospheres, 130, e2024JD042070,
864 https://doi.org/10.1029/2024JD042070, 2025.

865 Crawford, J. H., Ahn, J.-Y., Al-Saadi, J., Chang, L., Emmons, L. K., Kim, J., Lee, G., Park, J.-H., Park, R. J., Woo, J. H.,
866 Song, C.-K., Hong, J.-H., Hong, Y.-D., Lefer, B. L., Lee, M., Lee, T., Kim, S., Min, K.-E., Yum, S. S., Shin, H. J., Kim, Y.-
867 W., Choi, J.-S., Park, J.-S., Szykman, J. J., Long, R. W., Jordan, C. E., Simpson, I. J., Fried, A., Dibb, J. E., Cho, S., and Kim,
868 Y. P.: The Korea–United States Air Quality (KORUS-AQ) field study, Elementa: Science of the Anthropocene, 9, 00163,
869 https://doi.org/10.1525/elementa.2020.00163, 2021.

870 Crippa, M., Janssens-Maenhout, G., Guizzardi, D., Van Dingenen, R., and Dentener, F.: Contribution and uncertainty of
871 sectorial and regional emissions to regional and global $PM_{2.5}$ health impacts, Atmospheric Chemistry and Physics, 19, 5165–
872 5186, https://doi.org/10.5194/acp-19-5165-2019, 2019.

873 Crippa, M., Solazzo, E., Huang, G., Guizzardi, D., Koffi, E., Muntean, M., Schieberle, C., Friedrich, R., and Janssens-
874 Maenhout, G.: High resolution temporal profiles in the Emissions Database for Global Atmospheric Research, Sci Data, 7,
875 121, https://doi.org/10.1038/s41597-020-0462-2, 2020.

https://doi.org/10.5194/egusphere-2026-2380
Preprint. Discussion started: 8 May 2026

Crippa, M., Guizzardi, D., Butler, T., Keating, T., Wu, R., Kaminski, J., Kuenen, J., Kurokawa, J., Chatani, S., Morikawa, T., Pouliot, G., Racine, J., Moran, M. D., Klimont, Z., Manseau, P. M., Mashayekhi, R., Henderson, B. H., Smith, S. J., Suchyta, H., Muntean, M., Solazzo, E., Banja, M., Schaaf, E., Pagani, F., Woo, J.-H., Kim, J., Monforti-Ferrario, F., Pisoni, E., Zhang, J., Niemi, D., Sassi, M., Ansari, T., and Foley, K.: The HTAP_v3 emission mosaic: merging regional and global monthly emissions (2000–2018) to support air quality modelling and policies, Earth System Science Data, 15, 2667–2694, https://doi.org/10.5194/essd-15-2667-2023, 2023.

Crippa, M., Guizzardi, D., Pagani, F., Schiavina, M., Melchiorri, M., Pisoni, E., Graziosi, F., Muntean, M., Maes, J., Dijkstra, L., Van Damme, M., Clarisse, L., and Coheur, P.: Insights into the spatial distribution of global, national, and subnational greenhouse gas emissions in the Emissions Database for Global Atmospheric Research (EDGAR v8.0), Earth System Science Data, 16, 2811–2830, https://doi.org/10.5194/essd-16-2811-2024, 2024.

Cruz, M. T., Simpas, J. B., Sorooshian, A., Betito, G., Cambaliza, M. O. L., Collado, J. T., Eloranta, E. W., Holz, R., Topacio, X. G. V., Del Socorro, J., and Bagtasa, G.: Impacts of regional wind circulations on aerosol pollution and planetary boundary layer structure in Metro Manila, Philippines, Atmospheric Environment, 293, 119455, https://doi.org/10.1016/j.atmosenv.2022.119455, 2023.

Denier van der Gon, H., Gauss, M., Granier, C., Guevara, M., Arellano, S., Sindelarova, K., Liaskoni, M., Markova, J., Prieto Perez, A., Bartik, L., Jalkanen, J.-P., Majamäki, E., Quack, B., Bouarar, I., Li, C., Liousse, C., Simpson, D., Olivié, D., Benedictow, A., Segers, A., Zilbermann, N., Dellaert, S., Kuenen, J., Schoenmakers, E., Super, I., and Krueger, K.: Documentation of CAMS emission inventory products, https://doi.org/10.24380/UAG-0SVT, 2025.

De Smedt, I., Pinardi, G., Vigouroux, C., Compernolle, S., Bais, A., Benavent, N., Boersma, F., Chan, K.-L., Donner, S., Eichmann, K.-U., Hedelt, P., Hendrick, F., Irie, H., Kumar, V., Lambert, J.-C., Langerock, B., Lerot, C., Liu, C., Loyola, D., Piters, A., Richter, A., Rivera Cárdenas, C., Romahn, F., Ryan, R. G., Sinha, V., Theys, N., Vlietinck, J., Wagner, T., Wang, T., Yu, H., and Van Roozendael, M.: Comparative assessment of TROPOMI and OMI formaldehyde observations and validation against MAX-DOAS network column measurements, Atmospheric Chemistry and Physics, 21, 12561–12593, https://doi.org/10.5194/acp-21-12561-2021, 2021.

Deeter, M. N., Edwards, D. P., Francis, G. L., Gille, J. C., Martínez-Alonso, S., Worden, H. M., and Sweeney, C.: A climate-scale satellite record for carbon monoxide: the MOPITT Version 7 product, Atmospheric Measurement Techniques, 10, 2533–2555, https://doi.org/10.5194/amt-10-2533-2017, 2017.

Deng, Z., Ciais, P., Tzompa-Sosa, Z. A., Saunois, M., Qiu, C., Tan, C., Sun, T., Ke, P., Cui, Y., Tanaka, K., Lin, X., Thompson, R. L., Tian, H., Yao, Y., Huang, Y., Lauerwald, R., Jain, A. K., Xu, X., Bastos, A., Sitch, S., Palmer, P. I., Lauvaux, T., d'Aspremont, A., Giron, C., Benoit, A., Poulter, B., Chang, J., Petrescu, A. M. R., Davis, S. J., Liu, Z., Grassi, G., Albergel, C., Tubiello, F. N., Perugini, L., Peters, W., and Chevallier, F.: Comparing national greenhouse gas budgets reported in UNFCCC inventories against atmospheric inversions, Earth System Science Data, 14, 1639–1675, https://doi.org/10.5194/essd-14-1639-2022, 2022.

Ding, J., van der A, R., Mijling, B., de Laat, J., Eskes, H., and Boersma, K. F.: NOx emissions in India derived from OMI satellite observations, Atmospheric Environment: X, 14, 100174, https://doi.org/10.1016/j.aeaoa.2022.100174, 2022.

Diskin, G. S., Podolske, J. R., Sachse, G. W., and Slate, T. A.: Open-path airborne tunable diode laser hygrometer, in: Diode Lasers and Applications in Atmospheric Sensing, Diode Lasers and Applications in Atmospheric Sensing, 196–204, https://doi.org/10.1117/12.453736, 2002.

EANET: The Fourth Periodic Report on the State of Acid Deposition in East Asia (PRSAD4) - Part 3 - Executive Summary, 2021.

https://doi.org/10.5194/egusphere-2026-2380
Preprint. Discussion started: 8 May 2026

Elguindi, N., Granier, C., Stavrakou, T., Darras, S., Bauwens, M., Cao, H., Chen, C., Denier van der Gon, H. a. C., Dubovik, O., Fu, T. M., Henze, D. K., Jiang, Z., Keita, S., Kuenen, J. J. P., Kurokawa, J., Liousse, C., Miyazaki, K., Müller, J.-F., Qu, Z., Solmon, F., and Zheng, B.: Intercomparison of Magnitudes and Trends in Anthropogenic Surface Emissions From Bottom-Up Inventories, Top-Down Estimates, and Emission Scenarios, Earth's Future, 8, e2020EF001520, https://doi.org/10.1029/2020EF001520, 2020.

Energy Institute: Statistical Review of World Energy, 74th edition., Energy Institute, London, UK, 2025.

Field, R. D., van der Werf, G. R., and Shen, S. S. P.: Human amplification of drought-induced biomass burning in Indonesia since 1960, Nature Geosci, 2, 185–188, https://doi.org/10.1038/ngeo443, 2009.

Friedlingstein, P., O'Sullivan, M., Jones, M. W., Andrew, R. M., Bakker, D. C. E., Hauck, J., Landschützer, P., Le Quéré, C., Luijkx, I. T., Peters, G. P., Peters, W., Pongratz, J., Schwingshackl, C., Sitch, S., Canadell, J. G., Ciais, P., Jackson, R. B., Alin, S. R., Anthoni, P., Barbero, L., Bates, N. R., Becker, M., Bellouin, N., Decharme, B., Bopp, L., Brasika, I. B. M., Cadule, P., Chamberlain, M. A., Chandra, N., Chau, T.-T.-T., Chevallier, F., Chini, L. P., Cronin, M., Dou, X., Enyo, K., Evans, W., Falk, S., Feely, R. A., Feng, L., Ford, D. J., Gasser, T., Ghattas, J., Gkritzalis, T., Grassi, G., Gregor, L., Gruber, N., Gürses, Ö., Harris, I., Hefner, M., Heinke, J., Houghton, R. A., Hurtt, G. C., Iida, Y., Ilyina, T., Jacobson, A. R., Jain, A., Jarníková, T., Jersild, A., Jiang, F., Jin, Z., Joos, F., Kato, E., Keeling, R. F., Kennedy, D., Klein Goldewijk, K., Knauer, J., Korsbakken, J. I., Körtzinger, A., Lan, X., Lefèvre, N., Li, H., Liu, J., Liu, Z., Ma, L., Marland, G., Mayot, N., McGuire, P. C., McKinley, G. A., Meyer, G., Morgan, E. J., Munro, D. R., Nakaoka, S.-I., Niwa, Y., O'Brien, K. M., Olsen, A., Omar, A. M., Ono, T., Paulsen, M., Pierrot, D., Pocock, K., Poulter, B., Powis, C. M., Rehder, G., Resplandy, L., Robertson, E., Rödenbeck, C., Rosan, T. M., Schwinger, J., Séférian, R., et al.: Global Carbon Budget 2023, Earth System Science Data, 15, 5301–5369, https://doi.org/10.5194/essd-15-5301-2023, 2023.

Fu, D., Bowman, K. W., Worden, H. M., Natraj, V., Worden, J. R., Yu, S., Veefkind, P., Aben, I., Landgraf, J., Strow, L., and Han, Y.: High-resolution tropospheric carbon monoxide profiles retrieved from CrIS and TROPOMI, Atmospheric Measurement Techniques, 9, 2567–2579, https://doi.org/10.5194/amt-9-2567-2016, 2016.

Fu, D., Millet, D. B., Wells, K. C., Payne, V. H., Yu, S., Guenther, A., and Eldering, A.: Direct retrieval of isoprene from satellite-based infrared measurements, Nat Commun, 10, 3811, https://doi.org/10.1038/s41467-019-11835-0, 2019.

van Geffen, J., Eskes, H., Compernolle, S., Pinardi, G., Verhoelst, T., Lambert, J.-C., Sneep, M., ter Linden, M., Ludewig, A., Boersma, K. F., and Veefkind, J. P.: Sentinel-5P TROPOMI NO_2 retrieval: impact of version v2.2 improvements and comparisons with OMI and ground-based data, Atmospheric Measurement Techniques, 15, 2037–2060, https://doi.org/10.5194/amt-15-2037-2022, 2022.

Giglio, L., Randerson, J. T., and van der Werf, G. R.: Analysis of daily, monthly, and annual burned area using the fourth-generation global fire emissions database (GFED4), Journal of Geophysical Research: Biogeosciences, 118, 317–328, https://doi.org/10.1002/jgrg.20042, 2013.

Gopikrishnan, G. S. and Kuttippurath, J.: Four years of National Clean Air Programme (NCAP) in Indian cities: Assessment of the impact on surface ozone during the period 2018–2022, Sustainable Cities and Society, 101, 105207, https://doi.org/10.1016/j.scs.2024.105207, 2024.

Gopikrishnan, G. S., Ardra, T. S., and Kuttippurath, J.: Exposure to surface ozone and its associated health effects and economic burden in India, Global Transitions, 7, 148–158, https://doi.org/10.1016/j.glt.2025.03.002, 2025.

Graedel, T. E., Bates, T. S., Bouwman, A. F., Cunnold, D., Dignon, J., Fung, I., Jacob, D. J., Lamb, B. K., Logan, J. A., Marland, G., Middleton, P., Pacyna, J. M., Placet, M., and Veldt, C.: A compilation of inventories of emissions to the atmosphere, Global Biogeochemical Cycles, 7, 1–26, https://doi.org/10.1029/92GB02793, 1993.

https://doi.org/10.5194/egusphere-2026-2380
Preprint. Discussion started: 8 May 2026

Guenther, A. B., Jiang, X., Heald, C. L., Sakulyanontvittaya, T., Duhl, T., Emmons, L. K., and Wang, X.: The Model of Emissions of Gases and Aerosols from Nature version 2.1 (MEGAN2.1): an extended and updated framework for modeling biogenic emissions, Geoscientific Model Development, 5, 1471–1492, https://doi.org/10.5194/gmd-5-1471-2012, 2012.

Guevara, M., Jorba, O., Tena, C., Denier van der Gon, H., Kuenen, J., Elguindi, N., Darras, S., Granier, C., and Pérez García-Pando, C.: Copernicus Atmosphere Monitoring Service TEMPOral profiles (CAMS-TEMPO): global and European emission temporal profile maps for atmospheric chemistry modelling, Earth System Science Data, 13, 367–404, https://doi.org/10.5194/essd-13-367-2021, 2021.

Guizzardi, D., Crippa, M., Butler, T., Keating, T., Wu, R., Kaminski, J., Kuenen, J., Kurokawa, J., Chatani, S., Morikawa, T., Pouliot, G., Racine, J., Moran, M. D., Klimont, Z., Manseau, P. M., Mashayekhi, R., Henderson, B. H., Smith, S. J., Hoesly, R., Muntean, M., Banja, M., Schaaf, E., Pagani, F., Woo, J.-H., Kim, J., Pisoni, E., Zhang, J., Niemi, D., Sassi, M., Duhamel, A., Ansari, T., Foley, K., Geng, G., Chen, Y., and Zhang, Q.: The HTAP_v3.2 emission mosaic: merging regional and global monthly emissions (2000–2020) to support air quality modelling and policies, Earth System Science Data, 17, 5915–5950, https://doi.org/10.5194/essd-17-5915-2025, 2025.

Gurney, K. R., Liang, J., O'Keeffe, D., Patarasuk, R., Hutchins, M., Huang, J., Rao, P., and Song, Y.: Comparison of Global Downscaled Versus Bottom-Up Fossil Fuel CO_2 Emissions at the Urban Scale in Four U.S. Urban Areas, JGR Atmospheres, 124, 2823–2840, https://doi.org/10.1029/2018JD028859, 2019.

Guttikunda, S., Ka, N., Ganguly, T., and Jawahar, P.: Plugging the ambient air monitoring gaps in India's national clean air programme (NCAP) airsheds, Atmospheric Environment, 301, 119712, https://doi.org/10.1016/j.atmosenv.2023.119712, 2023.

Hannun, R. A., Swanson, A. K., Bailey, S. A., Hanisco, T. F., Bui, T. P., Bourgeois, I., Peischl, J., and Ryerson, T. B.: A cavity-enhanced ultraviolet absorption instrument for high-precision, fast-time-response ozone measurements, Atmospheric Measurement Techniques, 13, 6877–6887, https://doi.org/10.5194/amt-13-6877-2020, 2020.

Hersbach, H., Bell, B., Berrisford, P., Hirahara, S., Horányi, A., Muñoz-Sabater, J., Nicolas, J., Peubey, C., Radu, R., Schepers, D., Simmons, A., Soci, C., Abdalla, S., Abellan, X., Balsamo, G., Bechtold, P., Biavati, G., Bidlot, J., Bonavita, M., De Chiara, G., Dahlgren, P., Dee, D., Diamantakis, M., Dragani, R., Flemming, J., Forbes, R., Fuentes, M., Geer, A., Haimberger, L., Healy, S., Hogan, R. J., Hólm, E., Janisková, M., Keeley, S., Laloyaux, P., Lopez, P., Lupu, C., Radnoti, G., de Rosnay, P., Rozum, I., Vamborg, F., Villaume, S., and Thépaut, J.-N.: The ERA5 global reanalysis, Quarterly Journal of the Royal Meteorological Society, 146, 1999–2049, https://doi.org/10.1002/qj.3803, 2020.

Hoesly, R. M., Smith, S. J., Feng, L., Klimont, Z., Janssens-Maenhout, G., Pitkanen, T., Seibert, J. J., Vu, L., Andres, R. J., Bolt, R. M., Bond, T. C., Dawidowski, L., Kholod, N., Kurokawa, J., Li, M., Liu, L., Lu, Z., Moura, M. C. P., O'Rourke, P. R., and Zhang, Q.: Historical (1750–2014) anthropogenic emissions of reactive gases and aerosols from the Community Emissions Data System (CEDS), Geoscientific Model Development, 11, 369–408, https://doi.org/10.5194/gmd-11-369-2018, 2018.

Hopke, P. K., Cohen, D. D., Begum, B. A., Biswas, S. K., Ni, B., Pandit, G. G., Santoso, M., Chung, Y.-S., Davy, P., Markwitz, A., Waheed, S., Siddique, N., Santos, F. L., Pabroa, P. C. B., Seneviratne, M. C. S., Wimolwattanapun, W., Bunprapob, S., Vuong, T. B., Duy Hien, P., and Markowicz, A.: Urban air quality in the Asian region, Science of The Total Environment, 404, 103–112, https://doi.org/10.1016/j.scitotenv.2008.05.039, 2008.

Huang, M., Carmichael, G. R., Pierce, R. B., Jo, D. S., Park, R. J., Flemming, J., Emmons, L. K., Bowman, K. W., Henze, D. K., Davila, Y., Sudo, K., Jonson, J. E., Tronstad Lund, M., Janssens-Maenhout, G., Dentener, F. J., Keating, T. J., Oetjen, H., and Payne, V. H.: Impact of intercontinental pollution transport on North American ozone air pollution: an HTAP phase 2 multi-model study, Atmospheric Chemistry and Physics, 17, 5721–5750, https://doi.org/10.5194/acp-17-5721-2017, 2017.

https://doi.org/10.5194/egusphere-2026-2380
Preprint. Discussion started: 8 May 2026

Hunt, B. R., Kostelich, E. J., and Szunyogh, I.: Efficient data assimilation for spatiotemporal chaos: A local ensemble transform Kalman filter, Physica D: Nonlinear Phenomena, 230, 112–126, https://doi.org/10.1016/j.physd.2006.11.008, 2007.

Inness, A., Ades, M., Agustí-Panareda, A., Barré, J., Benedictow, A., Blechschmidt, A.-M., Dominguez, J. J., Engelen, R., Eskes, H., Flemming, J., Huijnen, V., Jones, L., Kipling, Z., Massart, S., Parrington, M., Peuch, V.-H., Razinger, M., Remy, S., Schulz, M., and Suttie, M.: The CAMS reanalysis of atmospheric composition, Atmospheric Chemistry and Physics, 19, 3515–3556, https://doi.org/10.5194/acp-19-3515-2019, 2019.

IPCC: 2006 IPCC Guidelines for National Greenhouse Gas Inventories – A primer, Prepared by the National Greenhouse Gas Inventories Programme, Eggleston H.S., Miwa K., Srivastava N. and Tanabe K. (eds)., Institute for Global Environmental Strategies (IGES), Hayama, Japan, 2008.

Itahashi, S., Ge, B., Sato, K., Fu, J. S., Wang, X., Yamaji, K., Nagashima, T., Li, J., Kajino, M., Liao, H., Zhang, M., Wang, Z., Li, M., Kurokawa, J., Carmichael, G. R., and Wang, Z.: MICS-Asia III: overview of model intercomparison and evaluation of acid deposition over Asia, Atmospheric Chemistry and Physics, 20, 2667–2693, https://doi.org/10.5194/acp-20-2667-2020, 2020.

Janssens-Maenhout, G., Crippa, M., Guizzardi, D., Muntean, M., Schaaf, E., Dentener, F., Bergamaschi, P., Pagliari, V., Olivier, J. G. J., Peters, J. A. H. W., van Aardenne, J. A., Monni, S., Doering, U., Petrescu, A. M. R., Solazzo, E., and Oreggioni, G. D.: EDGAR v4.3.2 Global Atlas of the three major greenhouse gas emissions for the period 1970–2012, Earth System Science Data, 11, 959–1002, https://doi.org/10.5194/essd-11-959-2019, 2019.

Jeong, D., Hornbrook, R. S., Hills, A. J., Diskin, G., Halliday, H. S., DiGangi, J. P., Fried, A., Richter, D., Walega, J., Weibring, P., Hanisco, T. F., Wolfe, G. M., St. Clair, J., Peischl, J., Wisthaler, A., Mikoviny, T., Nowak, J. B., Piel, F., Tomsche, L., Holmes, C. D., Soja, A., Gargulinski, E., Crawford, J. H., Dibb, J., Warneke, C., Schwarz, J., and Apel, E. C.: Trace Organic Gas Analyzer Time-of-Flight mass spectrometer (TOGA-TOF) system for airborne observations of formaldehyde, EGUsphere, 1–34, https://doi.org/10.5194/egusphere-2025-4703, 2025.

Kaiser, J. W., Heil, A., Andreae, M. O., Benedetti, A., Chubarova, N., Jones, L., Morcrette, J.-J., Razinger, M., Schultz, M. G., Suttie, M., and van der Werf, G. R.: Biomass burning emissions estimated with a global fire assimilation system based on observed fire radiative power, Biogeosciences, 9, 527–554, https://doi.org/10.5194/bg-9-527-2012, 2012.

Kim, J., Jeong, U., Ahn, M.-H., Kim, J. H., Park, R. J., Lee, H., Song, C. H., Choi, Y.-S., Lee, K.-H., Yoo, J.-M., Jeong, M.-J., Park, S. K., Lee, K.-M., Song, C.-K., Kim, S.-W., Kim, Y. J., Kim, S.-W., Kim, M., Go, S., Liu, X., Chance, K., Miller, C. C., Al-Saadi, J., Veihelmann, B., Bhartia, P. K., Torres, O., Abad, G. G., Haffner, D. P., Ko, D. H., Lee, S. H., Woo, J.-H., Chong, H., Park, S. S., Nicks, D., Choi, W. J., Moon, K.-J., Cho, A., Yoon, J., Kim, S., Hong, H., Lee, K., Lee, H., Lee, S., Choi, M., Veefkind, P., Levelt, P. F., Edwards, D. P., Kang, M., Eo, M., Bak, J., Baek, K., Kwon, H.-A., Yang, J., Park, J., Han, K. M., Kim, B.-R., Shin, H.-W., Choi, H., Lee, E., Chong, J., Cha, Y., Koo, J.-H., Irie, H., Hayashida, S., Kasai, Y., Kanaya, Y., Liu, C., Lin, J., Crawford, J. H., Carmichael, G. R., Newchurch, M. J., Lefer, B. L., Herman, J. R., Swap, R. J., Lau, A. K. H., Kurosu, T. P., Jaross, G., Ahlers, B., Dobber, M., McElroy, C. T., and Choi, Y.: New Era of Air Quality Monitoring from Space: Geostationary Environment Monitoring Spectrometer (GEMS), https://doi.org/10.1175/BAMS-D-18-0013.1, 2020.

Kim, Y. P. and Lee, G.: Trend of Air Quality in Seoul: Policy and Science, Aerosol Air Qual. Res., 18, 2141–2156, https://doi.org/10.4209/aaqr.2018.03.0081, 2018.

Kittipornkul, P., Thiravetyan, P., Hoshika, Y., Sorrentino, B., Popa, I., Leca, S., Sicard, P., Paoletti, E., and De Marco, A.: Surface ozone risk to human health and vegetation in tropical region: The case of Thailand, Environmental Research, 234, 116566, https://doi.org/10.1016/j.envres.2023.116566, 2023.

https://doi.org/10.5194/egusphere-2026-2380
Preprint. Discussion started: 8 May 2026

Koster, R. D., Darmenov, A., and Silva, A.: The Quick Fire Emissions Dataset (QFED): Documentation of Versions 2.1, 2.2 and 2.4. Volume 38; Technical Report Series on Global Modeling and Data Assimilation, 2015.

Kurokawa, J. and Ohara, T.: Long-term historical trends in air pollutant emissions in Asia: Regional Emission inventory in ASia (REAS) version 3, Atmospheric Chemistry and Physics, 20, 12761–12793, https://doi.org/10.5194/acp-20-12761-2020, 2020.

Kwon, H.-A., Park, R. J., González Abad, G., Chance, K., Kurosu, T. P., Kim, J., De Smedt, I., Van Roozendael, M., Peters, E., and Burrows, J.: Description of a formaldehyde retrieval algorithm for the Geostationary Environment Monitoring Spectrometer (GEMS), Atmospheric Measurement Techniques, 12, 3551–3571, https://doi.org/10.5194/amt-12-3551-2019, 2019.

Lahoz, W. A. and Schneider, P.: Data assimilation: making sense of Earth Observation, Front. Environ. Sci., 2, https://doi.org/10.3389/fenvs.2014.00016, 2014.

Langford, B., Misztal, P. K., Nemitz, E., Davison, B., Helfter, C., Pugh, T. a. M., MacKenzie, A. R., Lim, S. F., and Hewitt, C. N.: Fluxes and concentrations of volatile organic compounds from a South-East Asian tropical rainforest, Atmospheric Chemistry and Physics, 10, 8391–8412, https://doi.org/10.5194/acp-10-8391-2010, 2010.

Lawrence, M. G. and Lelieveld, J.: Atmospheric pollutant outflow from southern Asia: a review, Atmospheric Chemistry and Physics, 10, 11017–11096, https://doi.org/10.5194/acp-10-11017-2010, 2010.

Lee, G. T., Park, R. J., Kwon, H.-A., Ha, E. S., Lee, S. D., Shin, S., Ahn, M.-H., Kang, M., Choi, Y.-S., Kim, G., Lee, D.-W., Kim, D.-R., Hong, H., Langerock, B., Vigouroux, C., Lerot, C., Hendrick, F., Pinardi, G., De Smedt, I., Van Roozendael, M., Wang, P., Chong, H., Cho, Y., and Kim, J.: First evaluation of the GEMS formaldehyde product against TROPOMI and ground-based column measurements during the in-orbit test period, Atmospheric Chemistry and Physics, 24, 4733–4749, https://doi.org/10.5194/acp-24-4733-2024, 2024.

Lelieveld, J., Crutzen, P. J., Ramanathan, V., Andreae, M. O., Brenninkmeijer, C. A. M., Campos, T., Cass, G. R., Dickerson, R. R., Fischer, H., de Gouw, J. A., Hansel, A., Jefferson, A., Kley, D., de Laat, A. T. J., Lal, S., Lawrence, M. G., Lobert, J. M., Mayol-Bracero, O. L., Mitra, A. P., Novakov, T., Oltmans, S. J., Prather, K. A., Reiner, T., Rodhe, H., Scheeren, H. A., Sikka, D., and Williams, J.: The Indian Ocean Experiment: Widespread Air Pollution from South and Southeast Asia, Science, 291, 1031–1036, https://doi.org/10.1126/science.1057103, 2001.

Knez, L., Eckl, M., Waldmann, P., Fiehn, A., Pühl, M., Aseev, O., Diskin, G. S., DiGangi, J. P., Choi, Y., Miech, J. A., Bennett, R., Gatebe, C. K., Dean-Day, J. M., Poudyal, R., Lee, G., Kim, J., and Roiger, A.: Airborne performance assessment of the DLR MIRO MGA^3 quantum cascade laser spectrometer for fast N_2O measurements, EGUsphere, 1–36, https://doi.org/10.5194/egusphere-2026-1686, 2026.

Levelt, P. F., Joiner, J., Tamminen, J., Veefkind, J. P., Bhartia, P. K., Stein Zweers, D. C., Duncan, B. N., Streets, D. G., Eskes, H., van der A, R., McLinden, C., Fioletov, V., Carn, S., de Laat, J., DeLand, M., Marchenko, S., McPeters, R., Ziemke, J., Fu, D., Liu, X., Pickering, K., Apituley, A., González Abad, G., Arola, A., Boersma, F., Chan Miller, C., Chance, K., de Graaf, M., Hakkarainen, J., Hassinen, S., Ialongo, I., Kleipool, Q., Krotkov, N., Li, C., Lamsal, L., Newman, P., Nowlan, C., Suleiman, R., Tilstra, L. G., Torres, O., Wang, H., and Wargan, K.: The Ozone Monitoring Instrument: overview of 14 years in space, Atmospheric Chemistry and Physics, 18, 5699–5745, https://doi.org/10.5194/acp-18-5699-2018, 2018.

https://doi.org/10.5194/egusphere-2026-2380
Preprint. Discussion started: 8 May 2026

Li, M., Kurokawa, J., Zhang, Q., Woo, J.-H., Morikawa, T., Chatani, S., Lu, Z., Song, Y., Geng, G., Hu, H., Kim, J., Cooper, O. R., and McDonald, B. C.: MIXv2: a long-term mosaic emission inventory for Asia (2010–2017), Atmos. Chem. Phys., 24, 3925–3952, https://doi.org/10.5194/acp-24-3925-2024, 2024.

Liu, F., Zhang, Q., Tong, D., Zheng, B., Li, M., Huo, H., and He, K. B.: High-resolution inventory of technologies, activities, and emissions of coal-fired power plants in China from 1990 to 2010, Atmospheric Chemistry and Physics, 15, 13299–13317, https://doi.org/10.5194/acp-15-13299-2015, 2015.

Liu, T., Mickley, L. J., Marlier, M. E., DeFries, R. S., Khan, M. F., Latif, M. T., and Karambelas, A.: Diagnosing spatial biases and uncertainties in global fire emissions inventories: Indonesia as regional case study, Remote Sensing of Environment, 237, 111557, https://doi.org/10.1016/j.rse.2019.111557, 2020.

Liu, Y., Geng, G., Cheng, J., Liu, Y., Xiao, Q., Liu, L., Shi, Q., Tong, D., He, K., and Zhang, Q.: Drivers of Increasing Ozone during the Two Phases of Clean Air Actions in China 2013–2020, Environ. Sci. Technol., 57, 8954–8964, https://doi.org/10.1021/acs.est.3c00054, 2023.

Livesey, N. J., Filipiak, M. J., Froidevaux, L., Read, W. G., Lambert, A., Santee, M. L., Jiang, J. H., Pumphrey, H. C., Waters, J. W., Cofield, R. E., Cuddy, D. T., Daffer, W. H., Drouin, B. J., Fuller, R. A., Jarnot, R. F., Jiang, Y. B., Knosp, B. W., Li, Q. B., Perun, V. S., Schwartz, M. J., Snyder, W. V., Stek, P. C., Thurstans, R. P., Wagner, P. A., Avery, M., Browell, E. V., Cammas, J.-P., Christensen, L. E., Diskin, G. S., Gao, R.-S., Jost, H.-J., Loewenstein, M., Lopez, J. D., Nedelec, P., Osterman, G. B., Sachse, G. W., and Webster, C. R.: Validation of Aura Microwave Limb Sounder O3 and CO observations in the upper troposphere and lower stratosphere, Journal of Geophysical Research: Atmospheres, 113, https://doi.org/10.1029/2007JD008805, 2008.

Maneenoi, N., Saide, P. E., Christopoulos, J., Mohanty, M. R., Emmons, L., Tang, W., Buchholz, R. R., Wiedinmyer, C., and Boonlerd, V.: Geostationary Himawari-9 reveals missing agricultural burning outside LEO satellite detection windows and improves burned-area estimates in mainland Southeast Asia., Submitted to Atmospheric Environment.

Marlier, M. E., DeFries, R. S., Kim, P. S., Koplitz, S. N., Jacob, D. J., Mickley, L. J., and Myers, S. S.: Fire emissions and regional air quality impacts from fires in oil palm, timber, and logging concessions in Indonesia, Environ. Res. Lett., 10, 085005, https://doi.org/10.1088/1748-9326/10/8/085005, 2015.

Martin, R. V., Brauer, M., van Donkelaar, A., Shaddick, G., Narain, U., and Dey, S.: No one knows which city has the highest concentration of fine particulate matter, Atmospheric Environment: X, 3, 100040, https://doi.org/10.1016/j.aeaoa.2019.100040, 2019.

Marvin, M. R., Palmer, P. I., Yao, F., Latif, M. T., and Khan, M. F.: Uncertainties from biomass burning aerosols in air quality models obscure public health impacts in Southeast Asia, Atmospheric Chemistry and Physics, 24, 3699–3715, https://doi.org/10.5194/acp-24-3699-2024, 2024.

Mettig, N., Weber, M., Rozanov, A., Burrows, J. P., Veefkind, P., Thompson, A. M., Stauffer, R. M., Leblanc, T., Ancellet, G., Newchurch, M. J., Kuang, S., Kivi, R., Tully, M. B., Van Malderen, R., Piters, A., Kois, B., Stübi, R., and Skrivankova, P.: Combined UV and IR ozone profile retrieval from TROPOMI and CrIS measurements, Atmospheric Measurement Techniques, 15, 2955–2978, https://doi.org/10.5194/amt-15-2955-2022, 2022.

Miech, J. A., DiGangi, J. P., Diskin, G. S., Choi, Y., Moore, R. H., Ziemba, L. D., Gallo, F., Jordan, C. E., Shook, M. A., Wiggins, E. B., Winstead, E. L., Roy, S., Lee, Y. R., Ball, K., Crounse, J. D., Wennberg, P., Piel, F., Swift, S., Wojnowski, W., and Wisthaler, A.: Technical note: Identifying biomass burning emissions during ASIA-AQ using greenhouse gas

enhancement ratios, Atmospheric Chemistry and Physics, 25, 15701–15714, https://doi.org/10.5194/acp-25-15701-2025, 2025.

Miyazaki, K., Eskes, H. J., and Sudo, K.: Global NO_x emission estimates derived from an assimilation of OMI tropospheric NO_2 columns, Atmospheric Chemistry and Physics, 12, 2263–2288, https://doi.org/10.5194/acp-12-2263-2012, 2012.

Miyazaki, K., Eskes, H. J., and Sudo, K.: A tropospheric chemistry reanalysis for the years 2005–2012 based on an assimilation of OMI, MLS, TES, and MOPITT satellite data, Atmospheric Chemistry and Physics, 15, 8315–8348, https://doi.org/10.5194/acp-15-8315-2015, 2015.

Miyazaki, K., Bowman, K., Sekiya, T., Eskes, H., Boersma, F., Worden, H., Livesey, N., Payne, V. H., Sudo, K., Kanaya, Y., Takigawa, M., and Ogochi, K.: Chemical Reanalysis Products. Jet Propulsion Laboratory, https://doi.org/10.25966/9qgv-fe81, 2019

Miyazaki, K., Bowman, K. W., Yumimoto, K., Walker, T., and Sudo, K.: Evaluation of a multi-model, multi-constituent assimilation framework for tropospheric chemical reanalysis, Atmospheric Chemistry and Physics, 20, 931–967, https://doi.org/10.5194/acp-20-931-2020, 2020a.

Miyazaki, K., Bowman, K., Sekiya, T., Eskes, H., Boersma, F., Worden, H., Livesey, N., Payne, V. H., Sudo, K., Kanaya, Y., Takigawa, M., and Ogochi, K.: Updated tropospheric chemistry reanalysis and emission estimates, TCR-2, for 2005–2018, Earth System Science Data, 12, 2223–2259, https://doi.org/10.5194/essd-12-2223-2020, 2020b.

Mizzi, A. P., Arellano Jr., A. F., Edwards, D. P., Anderson, J. L., and Pfister, G. G.: Assimilating compact phase space retrievals of atmospheric composition with WRF-Chem/DART: a regional chemical transport/ensemble Kalman filter data assimilation system, Geoscientific Model Development, 9, 965–978, https://doi.org/10.5194/gmd-9-965-2016, 2016.

Nikam, J., Archer, D., and Nopsert, C.: Air quality in Thailand: Understanding the regulatory context, Stockholm Environment Institute (SEI), Stockholm, Sweden, 2021.

Oak, Y. J., Jacob, D. J., Pendergrass, D. C., Dang, R., Colombi, N. K., Chong, H., Lee, S., Kuk, S. K., and Kim, J.: Air quality trends and regimes in South Korea inferred from 2015–2023 surface and satellite observations, Atmospheric Chemistry and Physics, 25, 3233–3252, https://doi.org/10.5194/acp-25-3233-2025, 2025.

Oda, T., Maksyutov, S., and Andres, R. J.: The Open-source Data Inventory for Anthropogenic CO_2, version 2016 (ODIAC2016): a global monthly fossil fuel CO_2 gridded emissions data product for tracer transport simulations and surface flux inversions, Earth System Science Data, 10, 87–107, https://doi.org/10.5194/essd-10-87-2018, 2018.

Oomen, G.-M., Müller, J.-F., Stavrakou, T., De Smedt, I., Blumenstock, T., Kivi, R., Makarova, M., Palm, M., Röhling, A., Té, Y., Vigouroux, C., Friedrich, M. M., Frieß, U., Hendrick, F., Merlaud, A., Piters, A., Richter, A., Van Roozendael, M., and Wagner, T.: Weekly derived top-down volatile-organic-compound fluxes over Europe from TROPOMI HCHO data from 2018 to 2021, Atmospheric Chemistry and Physics, 24, 449–474, https://doi.org/10.5194/acp-24-449-2024, 2024.

Pabroa, P. C. B., Racho, J. M. D., Jagonoy, A. M., Valdez, J. D. G., Bautista VII, A. T., Yee, J. R., Pineda, R., Manlapaz, J., Atanacio, A. J., Coronel, I. C. V., Salvador, C. M. G., and Cohen, D. D.: Characterization, source apportionment and associated health risk assessment of respirable air particulates in Metro Manila, Philippines, Atmospheric Pollution Research, 13, 101379, https://doi.org/10.1016/j.apr.2022.101379, 2022.

Pagano, T. S. and Durham, R. M.: Moderate Resolution Imaging Spectroradiometer (MODIS), in: Sensor Systems for the Early Earth Observing System Platforms, Sensor Systems for the Early Earth Observing System Platforms, 2–17, https://doi.org/10.1117/12.152835, 1993.

Pan, X., Chin, M., Kahn, R. A., Matsui, H., Takemura, T., Lin, M., Xie, Y., Kim, D., and Val Martin, M.: The sensitivity of smoke aerosol dispersion to smoke injection height and source-strength: a multi-model AeroCom study, Atmospheric Chemistry and Physics, 26, 171–196, https://doi.org/10.5194/acp-26-171-2026, 2026.

Payne, V. H., Kulawik, S. S., Fischer, E. V., Brewer, J. F., Huey, L. G., Miyazaki, K., Worden, J. R., Bowman, K. W., Hintsa, E. J., Moore, F., Elkins, J. W., and Juncosa Calahorrano, J.: Satellite measurements of peroxyacetyl nitrate from the Cross-Track Infrared Sounder: comparison with ATom aircraft measurements, Atmos. Meas. Tech., 15, 3497–3511, https://doi.org/10.5194/amt-15-3497-2022, 2022a.

Payne, V. H., Kulawik, S. S., Fischer, E. V., Brewer, J. F., Huey, L. G., Miyazaki, K., Worden, J. R., Bowman, K. W., Hintsa, E. J., Moore, F., Elkins, J. W., and Juncosa Calahorrano, J.: Satellite measurements of peroxyacetyl nitrate from the Cross-Track Infrared Sounder: comparison with ATom aircraft measurements, Atmospheric Measurement Techniques, 15, 3497–3511, https://doi.org/10.5194/amt-15-3497-2022, 2022b.

Peñuelas, J. and Staudt, M.: BVOCs and global change, Trends in Plant Science, 15, 133–144, https://doi.org/10.1016/j.tplants.2009.12.005, 2010.

Phairuang, W., Hata, M., and Furuuchi, M.: Influence of agricultural activities, forest fires and agro-industries on air quality in Thailand, Journal of Environmental Sciences, 52, 85–97, https://doi.org/10.1016/j.jes.2016.02.007, 2017.

Phairuang, W., Suwattiga, P., Chetiyanukornkul, T., Hongtieab, S., Limpaseni, W., Ikemori, F., Hata, M., and Furuuchi, M.: The influence of the open burning of agricultural biomass and forest fires in Thailand on the carbonaceous components in size-fractionated particles, Environmental Pollution, 247, 238–247, https://doi.org/10.1016/j.envpol.2019.01.001, 2019.

Reddington, C. L., Yoshioka, M., Balasubramanian, R., Ridley, D., Toh, Y. Y., Arnold, S. R., and Spracklen, D. V.: Contribution of vegetation and peat fires to particulate air pollution in Southeast Asia, Environ. Res. Lett., 9, 094006, https://doi.org/10.1088/1748-9326/9/9/094006, 2014.

Ren, J., Guo, F., and Xie, S.: Diagnosing ozone–NO_x–VOC sensitivity and revealing causes of ozone increases in China based on 2013–2021 satellite retrievals, Atmospheric Chemistry and Physics, 22, 15035–15047, https://doi.org/10.5194/acp-22-15035-2022, 2022.

Ridley, B. A., Grahek, F. E., and Walega, J. G.: A Small High-Sensitivity, Medium-Response Ozone Detector Suitable for Measurements from Light Aircraft, Journal of Atmospheric and Oceanic Technology, 9, 142–148, https://doi.org/10.1175/1520-0426(1992)009%3C0142:ASHSMR%3E2.0.CO;2, 1992.

Rijsdijk, P., Eskes, H., Dingemans, A., Boersma, K. F., Sekiya, T., Miyazaki, K., and Houweling, S.: Quantifying uncertainties in satellite NO_2 superobservations for data assimilation and model evaluation, Geoscientific Model Development, 18, 483–509, https://doi.org/10.5194/gmd-18-483-2025, 2025.

Salvador, C. M. G., Alindajao, A. D., Burdeos, K. B., Lavapiez, M. A. M., Yee, J. R., Bautista, A. T., Pabroa, P. C. B., and Capangpangan, R. Y.: Assessment of Impact of Meteorology and Precursor in Long-term Trends of PM and Ozone in a Tropical City, Aerosol Air Qual. Res., 22, 210269, https://doi.org/10.4209/aaqr.210269, 2021.

Santee, M. L., Lambert, A., Read, W. G., Livesey, N. J., Cofield, R. E., Cuddy, D. T., Daffer, W. H., Drouin, B. J., Froidevaux, L., Fuller, R. A., Jarnot, R. F., Knosp, B. W., Manney, G. L., Perun, V. S., Snyder, W. V., Stek, P. C., Thurstans, R. P., Wagner, P. A., Waters, J. W., Muscari, G., de Zafra, R. L., Dibb, J. E., Fahey, D. W., Popp, P. J., Marcy, T. P., Jucks, K. W., Toon, G. C., Stachnik, R. A., Bernath, P. F., Boone, C. D., Walker, K. A., Urban, J., and Murtagh, D.: Validation of the Aura Microwave Limb Sounder HNO3 measurements, Journal of Geophysical Research: Atmospheres, 112, https://doi.org/10.1029/2007JD008721, 2007.

https://doi.org/10.5194/egusphere-2026-2380
Preprint. Discussion started: 8 May 2026

Sekiya, T., Miyazaki, K., Ogochi, K., Sudo, K., and Takigawa, M.: Global high-resolution simulations of tropospheric nitrogen dioxide using CHASER V4.0, Geoscientific Model Development, 11, 959–988, https://doi.org/10.5194/gmd-11-959-2018, 2018.

Sekiya, T., Miyazaki, K., Ogochi, K., Sudo, K., Takigawa, M., Eskes, H., and Boersma, K. F.: Impacts of Horizontal Resolution on Global Data Assimilation of Satellite Measurements for Tropospheric Chemistry Analysis, Journal of Advances in Modeling Earth Systems, 13, e2020MS002180, https://doi.org/10.1029/2020MS002180, 2021.

Seo, S., Valks, P., Lutz, R., Heue, K.-P., Hedelt, P., Molina García, V., Loyola, D., Lee, H., and Kim, J.: Tropospheric NO_2 retrieval algorithm for geostationary satellite instruments: applications to GEMS, Atmospheric Measurement Techniques, 17, 6163–6191, https://doi.org/10.5194/amt-17-6163-2024, 2024.

Shephard, M. W. and Cady-Pereira, K. E.: Cross-track Infrared Sounder (CrIS) satellite observations of tropospheric ammonia, Atmospheric Measurement Techniques, 8, 1323–1336, https://doi.org/10.5194/amt-8-1323-2015, 2015.

Shephard, M. W., Dammers, E., Cady-Pereira, K. E., Kharol, S. K., Thompson, J., Gainariu-Matz, Y., Zhang, J., McLinden, C. A., Kovachik, A., Moran, M., Bittman, S., Sioris, C. E., Griffin, D., Alvarado, M. J., Lonsdale, C., Savic-Jovcic, V., and Zheng, Q.: Ammonia measurements from space with the Cross-track Infrared Sounder: characteristics and applications, Atmospheric Chemistry and Physics, 20, 2277–2302, https://doi.org/10.5194/acp-20-2277-2020, 2020.

Simpson, I. J., Blake, N. J., Barletta, B., Diskin, G. S., Fuelberg, H. E., Gorham, K., Huey, L. G., Meinardi, S., Rowland, F. S., Vay, S. A., Weinheimer, A. J., Yang, M., and Blake, D. R.: Characterization of trace gases measured over Alberta oil sands mining operations: 76 speciated C2–C10 volatile organic compounds (VOCs), CO2, CH4, CO, NO, NO2, NOy, O3 and SO2, Atmos. Chem. Phys., 10, 11931–11954, https://doi.org/10.5194/acp-10-11931-2010, 2010.

Simpson, I. J., Blake, D. R., Blake, N. J., Meinardi, S., Barletta, B., Hughes, S. C., Fleming, L. T., Crawford, J. H., Diskin, G. S., Emmons, L. K., Fried, A., Guo, H., Peterson, D. A., Wisthaler, A., Woo, J.-H., Barré, J., Gaubert, B., Kim, J., Kim, M. J., Kim, Y., Knote, C., Mikoviny, T., Pusede, S. E., Schroeder, J. R., Wang, Y., Wennberg, P. O., and Zeng, L.: Characterization, sources and reactivity of volatile organic compounds (VOCs) in Seoul and surrounding regions during KORUS-AQ, Elementa: Science of the Anthropocene, 8, 37, https://doi.org/10.1525/elementa.434, 2020.

Sindelarova, K., Granier, C., Bouarar, I., Guenther, A., Tilmes, S., Stavrakou, T., Müller, J.-F., Kuhn, U., Stefani, P., and Knorr, W.: Global data set of biogenic VOC emissions calculated by the MEGAN model over the last 30 years, Atmospheric Chemistry and Physics, 14, 9317–9341, https://doi.org/10.5194/acp-14-9317-2014, 2014.

Sindelarova, K., Markova, J., Simpson, D., Huszar, P., Karlicky, J., Darras, S., and Granier, C.: High-resolution biogenic global emission inventory for the time period 2000–2019 for air quality modelling, Earth System Science Data, 14, 251–270, https://doi.org/10.5194/essd-14-251-2022, 2022.

Skoulidou, I., Koukouli, M.-E., Manders, A., Segers, A., Karagkiozidis, D., Gratsea, M., Balis, D., Bais, A., Gerasopoulos, E., Stavrakou, T., van Geffen, J., Eskes, H., and Richter, A.: Evaluation of the LOTOS-EUROS NO_2 simulations using ground-based measurements and S5P/TROPOMI observations over Greece, Atmospheric Chemistry and Physics, 21, 5269–5288, https://doi.org/10.5194/acp-21-5269-2021, 2021.

Sokhi, R. S., Moussiopoulos, N., Baklanov, A., Bartzis, J., Coll, I., Finardi, S., Friedrich, R., Geels, C., Grönholm, T., Halenka, T., Ketzel, M., Maragkidou, A., Matthias, V., Moldanova, J., Ntziachristos, L., Schäfer, K., Suppan, P., Tsegas, G., Carmichael, G., Franco, V., Hanna, S., Jalkanen, J.-P., Velders, G. J. M., and Kukkonen, J.: Advances in air quality research – current and emerging challenges, Atmospheric Chemistry and Physics, 22, 4615–4703, https://doi.org/10.5194/acp-22-4615-2022, 2022.

https://doi.org/10.5194/egusphere-2026-2380
Preprint. Discussion started: 8 May 2026

Solazzo, E., Crippa, M., Guizzardi, D., Muntean, M., Choulga, M., and Janssens-Maenhout, G.: Uncertainties in the Emissions Database for Global Atmospheric Research (EDGAR) emission inventory of greenhouse gases, Atmospheric Chemistry and Physics, 21, 5655–5683, https://doi.org/10.5194/acp-21-5655-2021, 2021.

Song, W., Zhang, Y.-L., Zhang, Y., Cao, F., Rauber, M., Salazar, G., Kawichai, S., Prapamontol, T., and Szidat, S.: Is biomass burning always a dominant contributor of fine aerosols in upper northern Thailand?, Environment International, 168, 107466, https://doi.org/10.1016/j.envint.2022.107466, 2022.

Soulie, A., Granier, C., Darras, S., Zilbermann, N., Doumbia, T., Guevara, M., Jalkanen, J.-P., Keita, S., Liousse, C., Crippa, M., Guizzardi, D., Hoesly, R., and Smith, S. J.: Global anthropogenic emissions (CAMS-GLOB-ANT) for the Copernicus Atmosphere Monitoring Service simulations of air quality forecasts and reanalyses, Earth Syst. Sci. Data, 16, 2261–2279, https://doi.org/10.5194/essd-16-2261-2024, 2024.

Stavrakou, T., Müller, J.-F., Bauwens, M., De Smedt, I., Van Roozendael, M., Guenther, A., Wild, M., and Xia, X.: Isoprene emissions over Asia 1979–2012: impact of climate and land-use changes, Atmospheric Chemistry and Physics, 14, 4587–4605, https://doi.org/10.5194/acp-14-4587-2014, 2014.

Sukkhum, S., Lim, A., Ingviya, T., and Saelim, R.: Seasonal Patterns and Trends of Air Pollution in the Upper Northern Thailand from 2004 to 2018, Aerosol Air Qual. Res., 22, 210318, https://doi.org/10.4209/aaqr.210318, 2022.

Theys, N., Fioletov, V., Li, C., De Smedt, I., Lerot, C., McLinden, C., Krotkov, N., Griffin, D., Clarisse, L., Hedelt, P., Loyola, D., Wagner, T., Kumar, V., Innes, A., Ribas, R., Hendrick, F., Vlietinck, J., Brenot, H., and Van Roozendael, M.: A sulfur dioxide Covariance-Based Retrieval Algorithm (COBRA): application to TROPOMI reveals new emission sources, Atmospheric Chemistry and Physics, 21, 16727–16744, https://doi.org/10.5194/acp-21-16727-2021, 2021.

Thongsame, W., Henze, D. K., Barth, M., Pfister, G., Kumar, R., Macatangay, R., and Hassan Bran, S.: Source Attribution and Health Burden of PM2.5 in Mainland Thailand, GeoHealth, 9, e2024GH001315, https://doi.org/10.1029/2024GH001315, 2025.

Tseng, Y.-L., Wu, C.-H., Yuan, C.-S., Bagtasa, G., Yen, P.-H., and Cheng, P.-H.: Inter-comparison of chemical characteristics and source apportionment of PM2.5 at two harbors in the Philippines and Taiwan, Science of The Total Environment, 793, 148574, https://doi.org/10.1016/j.scitotenv.2021.148574, 2021.

UN: World Urbanization Prospects 2025: Summary of Results, UN DESA/POP/2025/TR/ NO. 12. New York: United Nations, 2025.

UNEP: Air pollution in Asia and the Pacific: science-based solutions, United Nations Environment Programme (UNEP), Geneva, 2018.

UN.ESCAP: Asia-Pacific Regional Action Programme on Air Pollution: strengthening air quality standards and monitoring, 2025a.

UN.ESCAP: Success and challenges in addressing air pollution in North-East Asia : a call to strengthen regional collaboration, United Nations, 2025b.

UNIDO: International Yearbook of Industrial Statistics, 2025 edition., United Nations Industrial Development Organization (UNIDO), 2025.

Valin, L. C., Russell, A. R., Hudman, R. C., and Cohen, R. C.: Effects of model resolution on the interpretation of satellite NO_2 observations, Atmospheric Chemistry and Physics, 11, 11647–11655, https://doi.org/10.5194/acp-11-11647-2011, 2011.

https://doi.org/10.5194/egusphere-2026-2380
Preprint. Discussion started: 8 May 2026

Veefkind, J. P., Aben, I., McMullan, K., Förster, H., de Vries, J., Otter, G., Claas, J., Eskes, H. J., de Haan, J. F., Kleipool, Q., van Weele, M., Hasekamp, O., Hoogeveen, R., Landgraf, J., Snel, R., Tol, P., Ingmann, P., Voors, R., Kruizinga, B., Vink, R., Visser, H., and Levelt, P. F.: TROPOMI on the ESA Sentinel-5 Precursor: A GMES mission for global observations of the atmospheric composition for climate, air quality and ozone layer applications, Remote Sensing of Environment, 120, 70–83, https://doi.org/10.1016/j.rse.2011.09.027, 2012.

Verma, R. L., Oanh, N. T. K., Winijkul, E., Huy, L. N., Armart, I. P., Laowagul, W., Sooktawee, S., Permadi, D. A., Khan, M. F., Gunawardhana, L., and Patdu, M. K.: Air quality management status and needs of countries in South Asia and Southeast Asia, APN Science Bulletin, https://doi.org/10.30852/sb.2023.2222, 2023.

Vongruang, P., Wongwises, P., and Pimonsree, S.: Assessment of fire emission inventories for simulating particulate matter in Upper Southeast Asia using WRF-CMAQ, Atmospheric Pollution Research, 8, 921–929, https://doi.org/10.1016/j.apr.2017.03.004, 2017.

Watanabe, S., Hajima, T., Sudo, K., Nagashima, T., Takemura, T., Okajima, H., Nozawa, T., Kawase, H., Abe, M., Yokohata, T., Ise, T., Sato, H., Kato, E., Takata, K., Emori, S., and Kawamiya, M.: MIROC-ESM 2010: model description and basic results of CMIP5-20c3m experiments, Geoscientific Model Development, 4, 845–872, https://doi.org/10.5194/gmd-4-845-2011, 2011.

Wells, K. C., Millet, D. B., Payne, V. H., Deventer, M. J., Bates, K. H., de Gouw, J. A., Graus, M., Warneke, C., Wisthaler, A., and Fuentes, J. D.: Satellite isoprene retrievals constrain emissions and atmospheric oxidation, Nature, 585, 225–233, https://doi.org/10.1038/s41586-020-2664-3, 2020.

Wells, K. C., Millet, D. B., Payne, V. H., Vigouroux, C., Aquino, C. A. B., De Mazière, M., De Gouw, J. A., Graus, M., Kurosu, T., Warneke, C., and Wisthaler, A.: Next-Generation Isoprene Measurements From Space: Detecting Daily Variability at High Resolution, JGR Atmospheres, 127, e2021JD036181, https://doi.org/10.1029/2021JD036181, 2022.

Wells, K. C., Millet, D. B., Brewer, J. F., Payne, V. H., Cady-Pereira, K. E., Pernak, R., Kulawik, S., Vigouroux, C., Jones, N., Mahieu, E., Makarova, M., Nagahama, T., Ortega, I., Palm, M., Strong, K., Schneider, M., Smale, D., Sussmann, R., and Zhou, M.: Global decadal measurements of methanol, ethene, ethyne, and HCN from the Cross-track Infrared Sounder, Atmospheric Measurement Techniques, 18, 695–716, https://doi.org/10.5194/amt-18-695-2025, 2025.

Wiedinmyer, C., Kimura, Y., McDonald-Buller, E. C., Emmons, L. K., Buchholz, R. R., Tang, W., Seto, K., Joseph, M. B., Barsanti, K. C., Carlton, A. G., and Yokelson, R.: The Fire Inventory from NCAR version 2.5: an updated global fire emissions model for climate and chemistry applications, Geoscientific Model Development, 16, 3873–3891, https://doi.org/10.5194/gmd-16-3873-2023, 2023.

Worden, H. M., Francis, G. L., Kulawik, S. S., Bowman, K. W., Cady-Pereira, K., Fu, D., Hegarty, J. D., Kantchev, V., Luo, M., Payne, V. H., Worden, J. R., Commane, R., and McKain, K.: TROPESS/CrIS carbon monoxide profile validation with NOAA GML and ATom in situ aircraft observations, Atmospheric Measurement Techniques, 15, 5383–5398, https://doi.org/10.5194/amt-15-5383-2022, 2022.

Wu, N., Geng, G., Xu, R., Liu, S., Liu, X., Shi, Q., Zhou, Y., Zhao, Y., Liu, H., Song, Y., Zheng, J., Zhang, Q., and He, K.: Development of a high-resolution integrated emission inventory of air pollutants for China, Earth Syst. Sci. Data, 16, 2893–2915, https://doi.org/10.5194/essd-16-2893-2024, 2024.

Yang, B., Wiser, F. C., McNeill, V. F., Fiore, A. M., Tao, M., Henze, D. K., Sen, S., and Westervelt, D. M.: Implementation and evaluation of the automated model reduction (AMORE) version 1.1 isoprene oxidation mechanism in GEOS-Chem, Environ. Sci.: Atmos., 3, 1820–1833, https://doi.org/10.1039/D3EA00121K, 2023.

https://doi.org/10.5194/egusphere-2026-2380
Preprint. Discussion started: 8 May 2026

Yang, L. H., Jacob, D. J., Dang, R., Oak, Y. J., Lin, H., Kim, J., Zhai, S., Colombi, N. K., Pendergrass, D. C., Beaudry, E., Shah, V., Feng, X., Yantosca, R. M., Chong, H., Park, J., Lee, H., Lee, W.-J., Kim, S., Kim, E., Travis, K. R., Crawford, J. H., and Liao, H.: Interpreting Geostationary Environment Monitoring Spectrometer (GEMS) geostationary satellite observations of the diurnal variation in nitrogen dioxide (NO_2) over East Asia, Atmospheric Chemistry and Physics, 24, 7027–7039, https://doi.org/10.5194/acp-24-7027-2024, 2024.

Yoon, J. (Young S., Wells, K. C., Millet, D. B., Swann, A. L. S., Thornton, J., and Turner, A. J.: Impacts of Interannual Isoprene Variations on Methane Lifetimes and Trends, Geophysical Research Letters, 52, e2025GL114712, https://doi.org/10.1029/2025GL114712, 2025.

Zhang, Q., Zheng, Y., Tong, D., Shao, M., Wang, S., Zhang, Y., Xu, X., Wang, J., He, H., Liu, W., Ding, Y., Lei, Y., Li, J., Wang, Z., Zhang, X., Wang, Y., Cheng, J., Liu, Y., Shi, Q., Yan, L., Geng, G., Hong, C., Li, M., Liu, F., Zheng, B., Cao, J., Ding, A., Gao, J., Fu, Q., Huo, J., Liu, B., Liu, Z., Yang, F., He, K., and Hao, J.: Drivers of improved PM2.5 air quality in China from 2013 to 2017, Proc Natl Acad Sci U S A, 116, 24463–24469, https://doi.org/10.1073/pnas.1907956116, 2019.